1960

Nonlinear network analysis by iterated integrals

John Paul Pritchard Jr.
Iowa State University

NONLINEAR NETWORK ANALYSIS BY ITERATED INTEGRALS

by

John Paul Pritchard, Jr.

A Dissertation Submitted to the
Graduate Faculty in Partial Fulfillment of
The Requirements for the Degree of
DOCTOR OF PHILOSOPHY

Major Subject: Electrical Engineering

Approved:

Signature was redacted for privacy.

In Charge of Major Work

Signature was redacted for privacy.

Head of Major Department

Signature was redacted for privacy.

Dean of Graduate College

Iowa State University
Of Science and Technology
Ames, Iowa

1960

TABLE OF CONTENTS

INTRODUCTION

The intent of this paper is the development of a general method for the transient and limited steady state analysis of electrical networks containing lumped parameter elements, some of which possess nonlinear characteristics. The resulting technique offers a methodical approach to such an analysis, producing a set of integral equations from the mesh or nodal equations of the given network. This set of integral equations implicitly defines the dependent variables and will require iterative means to solve for these explicitly.

When the proposed iterative approach is convergent, there results a set of transient solutions for these variables. Information concerning the steady state response of the network under an assumed excitation may be obtained in some cases by extending the transient solution over a sufficiently long time interval. Since the final iterative solution of the integral equations will be performed numerically, the total time span for which the solution possesses any desired degree of accuracy is restricted by the accumulative errors inherent in the numerical approach. This is remedied in part by adopting a greater resolution in the time increment used for the approximations.

The proposed method requires the performance of extensive numerical calculations when applied to the analysis of

practical networks. Through the use of digital computers this data processing requirement can be reduced to a rapidly performed detail in the overall analysis scheme. This use of a computing medium implies the need for a concise, well ordered means of presenting information to the computer. In addition, the operations to be performed should be organized so that the computer program developed may be as general as possible, and requires a minimum of modification for the analysis of a variety of similar problems. These considerations are not to imply a treatise on computing techniques, but in themselves have strongly influenced the author in the manner of formulating the material.

The network analysis notation used is given in Bode (2) and the principles of Laplace transform theory employed are treated extensively in Gardner and Barnes (3). Standard principles of numerical analysis have been adapted to the present need.

THE NETWORK SOLUTION AS A SET OF INTEGRAL EQUATIONS

Initially, consider the equation set 1 representing the mesh analysis of the general passive network appearing in Figure 1.

$$\begin{aligned} e_1(t) &= z_{11}i_1(t) - z_{12}i_2(t) - z_{13}i_3(t) , \\ e_2(t) &= - z_{21}i_1(t) + z_{22}i_2(t) - z_{23}i_3(t) , \\ e_3(t) &= - z_{31}i_1(t) - z_{32}i_2(t) + z_{33}i_3(t) , \end{aligned} \tag{1}$$

subject to the initial conditions

$$\begin{aligned} & i_j(0) , \\ & \int^{o} i_j(t)dt \triangleq q_j(0) \ ; \text{ for } j = 1, 2, 3. \end{aligned} \tag{2}$$

The z_{pj} are introduced for compactness and are linear operators defined as follows.

$$z_{pj} \triangleq L_{pj} \frac{d}{dt} + R_{pj} + C_{pj}^{-1} \int^{t} dt , \tag{3}$$

with $z_{pj} = z_{jp}$ for this example. The double subscript notation permits the distinction between the self or total characteristic of loop p if $p = j$ and the mutual or shared characteristic between loops p and j if $p \neq j$. For example, the self and mutual characteristics of loop 1 with respect to itself and the other loops of Figure 1 are

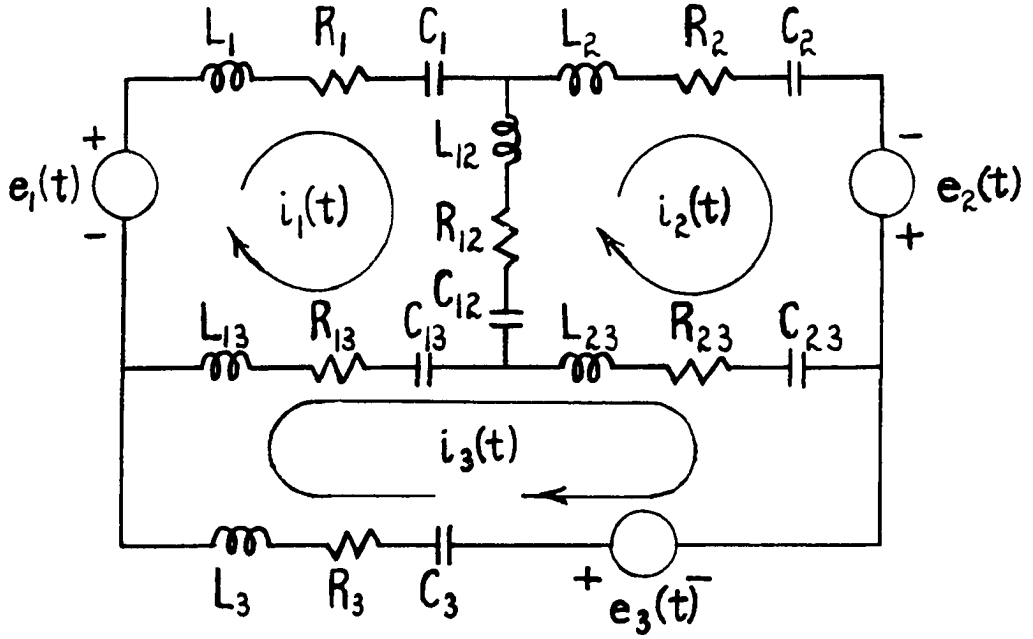

Figure 1. Linear electrical network for mesh analysis

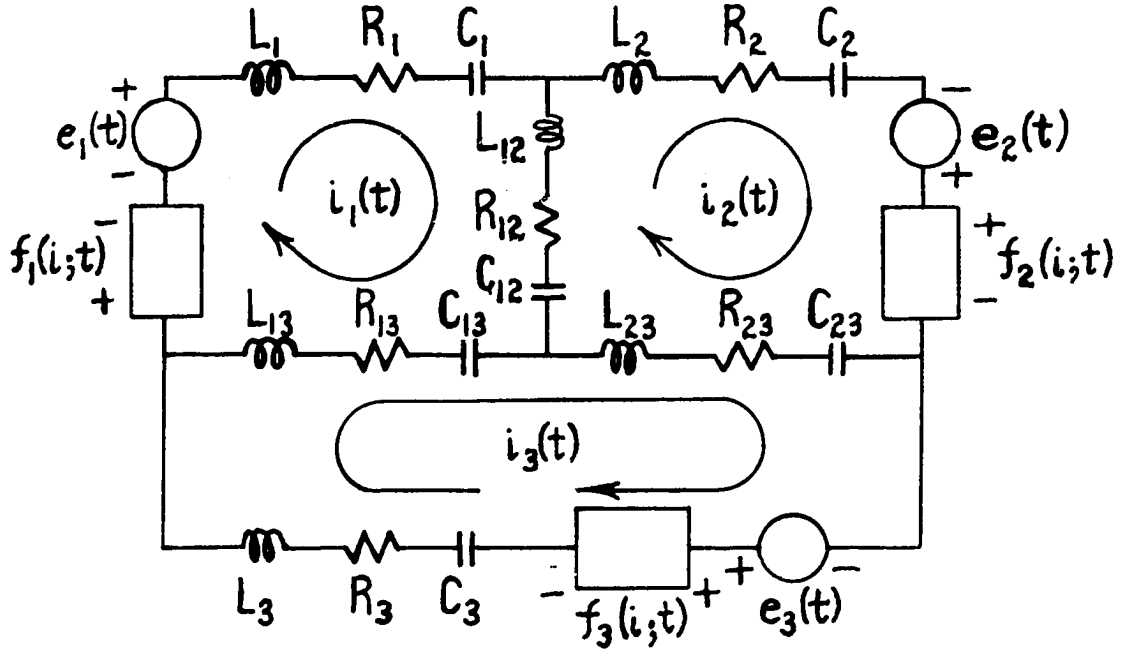

Figure 2. Network of Figure 1 augmented by nonlinear elements producing voltage drops $f_i(i;t)$ around loop i

$$R_{11} = R_1 + R_{12} + R_{13};\ R_{12} = R_{12};\ R_{13} = R_{13}\ ,$$
$$L_{11} = L_1 + L_{12} + L_{13};\ L_{12} = L_{12};\ L_{13} = L_{13}\ , \qquad (4)$$
$$C_{11}^{-1} = C_1^{-1} + C_{12}^{-1} + C_{13}^{-1};\ C_{12}^{-1} = C_{12}^{-1};\ C_{13}^{-1} = C_{13}^{-1}\ .$$

The $e_p(t)$ represents the total driving voltage encountered in passage around the mesh current loop designated by the subscript.

Assume now that the branches of the network of Figure 1 contain elements possessing nonlinear volt-ampere characteristics, the situation being as pictured in Figure 2. The symbol $f_p(i;t)$ represents the total voltage drop due to such nonlinear elements encountered in passage around loop p. These voltages are assumed to be functions of the currents $i = (i_1, i_2, i_3)$ with a fundamental dependence on the independent time variable t.

The only restriction placed on the $f_p(i;t)$ at this point is that they be functions which possess Laplace transforms. This requires that the functions be single valued and continuous nearly everywhere with respect to the time variable, and that there exists a real number σ_a such that

$$\mathcal{L}\left\{f(t)\right\} = \lim_{\substack{a\to 0 \\ T\to\infty}} \int_a^T \left|f_p(i;t)\right| e^{-\sigma_a t}\,dt < \infty\ . \qquad (5)$$

This same restriction is placed on the driving voltages.

The mesh equations for Figure 2 may be written in matrix form as

$$\begin{vmatrix} e_1(t) \\ e_2(t) \\ e_3(t) \end{vmatrix} = \begin{bmatrix} z_{11} & -z_{12} & -z_{13} \\ -z_{21} & z_{22} & -z_{23} \\ -z_{31} & -z_{32} & z_{33} \end{bmatrix} \begin{vmatrix} i_1(t) \\ i_2(t) \\ i_3(t) \end{vmatrix} + \begin{vmatrix} f_1(i;t) \\ f_2(i;t) \\ f_3(i;t) \end{vmatrix} , \quad (6)$$

or in more compact form

$$\left|e_p(t)\right| = \left[z_{pj}\right] \left|i_j(t)\right| + \left|f_p(i;t)\right| . \quad (7)$$

The Laplace transformation of equation 7, subject to the initial conditions of equation 2, is

$$\left|E_p(s)\right| = \left[Z_{pj}(s)\right] \left|I_j(s)\right| + \left|B_p(s)\right| + \left|F_p(I;s)\right| . \quad (8)$$

The symbols introduced in equation 8 are defined as follow.

$$E_p(s) = \mathcal{L}\left\{e_p(t)\right\} , \quad (9a)$$

$$I_j(s) = \mathcal{L}\left\{i_j(t)\right\} , \quad (9b)$$

$$Z_{pj}(s) = \mathcal{L}\left\{z_{pj}\right\} = sL_{pj} + R_{pj} + (sC_{pj})^{-1} , \quad (9c)$$

$$B_p(s) = -L_{pp}i_p(0) + (sC_{pp})^{-1}q_p(0) + \sum_{\substack{j=1 \\ j\neq p}}^{3} \left[L_{pj}i_j(0) - (sC_{pj})^{-1}q_j(0)\right] , \quad (9d)$$

$$F_p(I;s) = \mathcal{L}\left\{f_p(i;t)\right\} . \quad (9e)$$

To show that the transformation carries a term of the form $z_{pj}i_j(t)$, with zero initial conditions, into the defined form $Z_{pj}(s)I_j(s)$, consider

$$\mathcal{L}\left\{z_{pj}i_j(t)\right\} = \mathcal{L}\left\{L_{pj}\frac{di_j(t)}{dt} + R_{pj}i_j(t) + C_{pj}^{-1}\int^t i_j(t)dt\right\}$$

$$= \left\{sL_{pj} + R_{pj} + (sC_{pj})^{-1}\right\}\mathcal{L}\left\{i_j(t)\right\} \qquad (10)$$

$$= Z_{pj}(s)I_j(s) \ .$$

The addition of the $B_p(s)$ completes the description by including the effects of the actual initial conditions in the linear components of the network. The interpretation placed on the double subscript notation above permits the treatment of all linear initial conditions in this form.

A pseudo-driving function transform is defined as

$$E'_p(s) \triangleq E_p(s) - B_p(s) - F_p(I;s) \ . \qquad (11)$$

Then equation 8 becomes

$$\left[E'_p(s)\right] = \left[Z_{pj}(s)\right]\left[I_j(s)\right] . \qquad (12)$$

Equation 12 may now be solved for the linear occurrence of the instantaneous currents' transforms $I_j(s)$ by means of determinants, providing that the determinant of $\left[Z_{pj}(s)\right]$ is not identically zero. Proceeding in this manner, the transform of the current in the j^{th} mesh is given by

$$I_j(s) = \sum_{p=1}^{3} \frac{\Delta_{pj}(s)}{\Delta(s)} E'_p(s) \ , \qquad (13)$$

where $\Delta_{pj}(s)$ is the cofactor of the element $z_{pj}(s)$ in $\left[Z_{pj}(s)\right]$ and $\Delta(s)$ is the determinant of $\left[Z_{pj}(s)\right]$. In view

of the definition of the $z_{pj}(s)$ in terms of the linear characteristics of the network, it is noted that all terms of the form $\frac{\Delta_{pj}(s)}{\Delta(s)}$ may be reduced to the quotient of two polynomials in s. In the linearized network, these quantities are the transform expressions for the driving point admittance of the p^{th} loop for $j = p$, and the transfer admittance from the p^{th} loop to the j^{th} loop for $j \neq p$.

The currents i(t) in the time domain are obtained by the inverse Laplace transformation of the set of equations represented by equation 13. This inversion of the products of admittance and voltage transforms will be accomplished by real convolution. The theorem of real convolution states that: Given $G(s) = \mathcal{L}\{g(t)\}$ and $H(s) = \mathcal{L}\{h(t)\}$, then

$$\begin{aligned} \mathcal{L}^{-1}\{G(s)\cdot H(s)\} &\triangleq g(t)*h(t) \\ &= \int_0^t g(t-\lambda)h(\lambda)d\lambda \\ &= \int_0^t g(\lambda)h(t-\lambda)d\lambda . \end{aligned} \tag{14}$$

If the $\frac{\Delta_{pj}(s)}{\Delta(s)}$ are related to the G(s) and the $E'_p(s)$ to the H(s) of the equalities 14, the inverse transformation of equation 13 becomes

$$i_j(t) = \sum_{p=1}^{3} \int_0^t P_{pj}(t-\lambda)e'_p(\lambda)d\lambda , \tag{15}$$

where

$$P_{pj}(t) \triangleq \mathcal{L}^{-1}\left\{\frac{\Delta_{pj}(s)}{\Delta(s)}\right\} , \tag{16}$$

and

$$e'_p(t) = e_p(t) - b_p(t) - f_p(i;t) \quad . \tag{17}$$

In the absence of nonlinear elements, the $f_p(i;t)$ are zero and equation 15 may be solved for $i_j(t)$ without iteration. However, when the $f_p(i;t)$ do exist, the set of three equations, represented by equation 15, implicitly relate the three currents desired. The proposed method of solving this set of equations will be discussed later in this chapter and in the following chapter regarding iterative methods.

The quantities of equations 16 and 17 require further definition and discussion. Of the voltages in equation 17, the form of the excitation function $e_p(t)$ is arbitrary while that of the $f_p(i;t)$ will depend on the volt-ampere relationships for the nonlinearities present. The $b_p(t)$ may be expanded explicitly for the network of Figure 2 by inverse transformation of equation 9d.

$$b_p(t) = - L_{pp} i_p(0) u_1(t) + C_{pp}^{-1} q_p(0) u_0(t) + \sum_{\substack{j=1 \\ j \neq p}}^{3} \left[L_{pj} i_j(0) u_1(t) - C_{pj}^{-1} q_j(0) u_0(t) \right] \quad . \tag{18}$$

The $u_0(t)$ and $u_1(t)$ are the unit step and unit impulse respectively, as defined in Appendix A.

The admittance function $P_{pj}(t)$ may be generally described by

$$P_{pj}(t) = \sum_{h=1} B_h u_h(t) + u_0(t) \sum_{m=0} K_m t^{\rho_m} e^{\alpha_m t} \sin(\beta_m t + \phi_m) \ . \quad (19)$$

Since $\frac{\Delta_{pj}(s)}{\Delta(s)}$ is a rational function, it possesses a partial fraction expansion in terms of its finite poles in addition to a polynomial in s due to its infinite poles. This is shown generally in Ahlfors (1, pp. 44-45). A detailed study of the general inverse Laplace transformation of a rational function may be found in Gardner and Barnes (3, pp. 153-164, 255-257).

To identify the terms of equation 19, consider the admittance function transform

$$\frac{\Delta_{pj}(s)}{\Delta(s)} = \frac{C(s)}{D(s)} = \frac{c_4 s^4 + c_3 s^3 + c_2 s^2 + c_1 s + c_0}{s^3 + d_2 s^2 + d_1 s + d_0} \quad (20)$$

$$= c_4 s + (c_3 - c_4 d_2) + \frac{A(s)}{D(s)} \ ,$$

where A(s) is a quadratic remainder for the indicated division. The first identification to be made is

$$\mathcal{L}^{-1}\{c_4 s + (c_3 - c_4 d_2)\} = c_4 u_2(t) + (c_3 - c_4 d_2) u_1(t) \ , \quad (21)$$

as compared with the terms of equation 19,

$$\sum_{h=1} B_h u_h(t) = B_1 u_1(t) + B_2 u_2(t) + \ldots \ . \quad (22)$$

Equation 21 follows from the definition of the transform pairs

$$\mathcal{L}\{u_h(t)\} \triangleq s^{h-1} \ , \text{ for } h \geq 1 \ . \quad (23)$$

A more detailed description of these impulses and their properties appears in Appendix A.

To obtain the remaining series form of equation 19,

$$u_0(t)\sum_{m=0} K_m t^{\rho_m} e^{\alpha_m t} \sin(\beta_m t + \phi_m) \ , \qquad (24)$$

the proper fraction $\frac{A(s)}{D(s)}$ is expanded in partial fractions in terms of the roots $(\alpha_m + j\beta_m)$ of the characteristic polynomial D(s). Since D(s) has only real coefficients, its complex roots will occur in conjugate pairs. The inverse transformation of the partial fraction expansion is made term by term by referring to transform tables. For example, see Gardner and Barnes (3, pp. 332-356). The real coefficient K_m and the phase angle ϕ_m result by combining the functions of time corresponding to a pair of conjugate complex roots. For the real roots of D(s), this pairing of functions is not necessary to obtain a real coefficient K_m. Therefore ϕ_m, as well as β_m, is zero. The factor t^{ρ_m} is required if D(s) has multiple roots, where ρ_m is a positive integer.

The admittance function referred to is that of the linearized network and not descriptive of the actual network. As a result of the total omission of the elements with nonlinear characteristics, this linearized network may appear in a form generally inadmissable for analysis. For example, consider the simple situation of Figure 3. In this case,

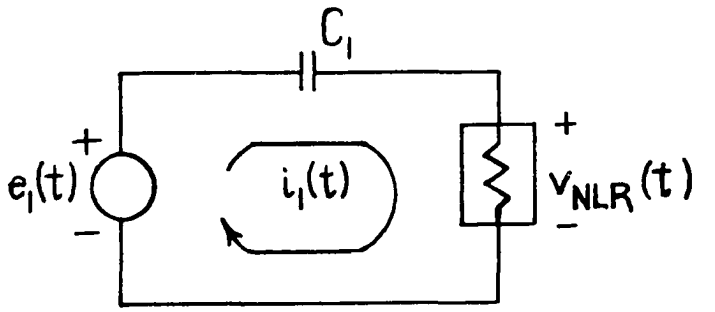

Figure 3. Illustrative network yielding a unit doublet in its admittance function

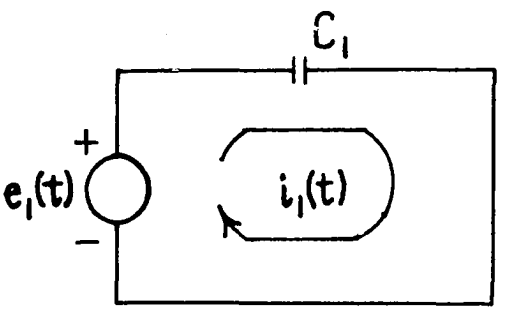

Figure 4. Linear portion of circuit of Figure 3

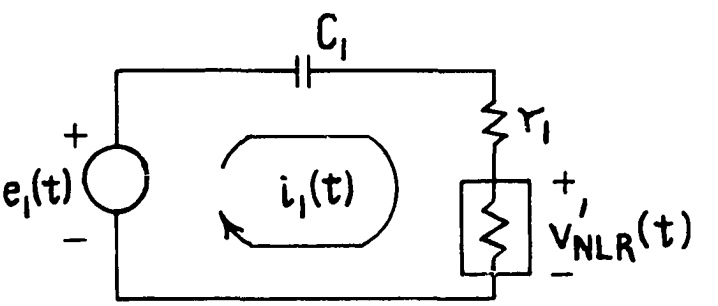

Figure 5. Alternative circuit description of Figure 3 without a unit doublet in its admittance function

the resistance possesses a nonlinear characteristic and, for the purpose of determining the admittance function, is omitted in Figure 4. The admittance transform is then

$$\frac{\Delta_{11}(s)}{\Delta(s)} = Cs \ , \tag{25}$$

or

$$\mathcal{L}\{P_{11}(t)\} = \mathcal{L}\{Cu_2(t)\} \ . \tag{26}$$

The choice of a driving voltage function is restricted by the fact that the voltage across a capacitor cannot change instantaneously. The verification of this follows from the principle of continuity of electric charge, q(t), where

$$q(t) \triangleq \int^t i(t)dt \ , \tag{27}$$

and upon Laplace transformation,

$$Q(s) = \frac{I(s)}{s} \ . \tag{28}$$

Assuming zero initial voltage across the capacitor of Figure 4, there follows from equation 13, with the admittance transform of equation 25,

$$\begin{aligned} Q_1(s) &= \frac{I_1(s)}{s} \\ &= \frac{1}{s}\frac{\Delta_{11}(s)}{\Delta(s)} E_1(s) \\ &= \frac{1}{s} CsE_1(s) \\ &= CE_1(s) \ . \end{aligned} \tag{29}$$

From the latter equality it is apparent that the continuity of $q_1(t)$ is exactly that of the $e_1(t)$ for all positive time, including the time origin. This eliminates the possibility of unit step and unit impulse driving voltages often assumed in analyzing transient responses. An analogous statement regarding the instantaneous change of current flow through an inductor arises in the nodal analysis of a linear system. This is based on the principle that magnetic flux density cannot change instantaneously.

When the unit doublet occurs in some admittance term $P_{pj}(t)$, two alternatives exist for resolving the problem without violation of physical principles. The first interpretation follows the lead offered in equation 29 and its discussion. This insists that the net effect of the $e'_p(t)$ represents a continuous function for all positive time, including the time origin. A second means of proceeding is through the redefinition of the nonlinear element or elements whose omission has produced the situation. For the example of Figure 3, this may be accomplished by assuming that the voltage induced in the nonlinear resistance may be represented as shown in Figure 5 by

$$v'_{NLR}(t) \triangleq f_1(i_1;t) = v_{NLR}(t) - r_1 i_1(t) , \quad (30)$$

where r_1 is some conveniently chosen constant resistance.

The occurrence of a unit impulse in an admittance ex-

pression causes no conflict with physical principles. This is observed by considering the simplest case of its occurrence, namely a single linear resistor R in series with a driving voltage $e_p(t)$. For this circuit, the admittance transform is simply R^{-1}. The loop current then, by equation 15, is

$$\begin{aligned} i_p(t) &= \mathcal{L}^{-1}\{R^{-1}E_p(s)\} \\ &= \int_0^t R^{-1}u_1(\lambda)e_p(t-\lambda)d\lambda \\ &\triangleq R^{-1}e_p(t) \ , \end{aligned} \tag{31}$$

with the aid of the impulse properties of Appendix A.

Impulses of order greater than the unit doublet cannot arise in the analysis of passive networks. To establish this point, the discussion of Figure 3 is recalled in which the existence of the unit doublet is found to violate physical principles. A direct implication of that result is the inability of a passive network to differentiate exactly. This follows from the fact that the linear operator $\frac{d}{dt}$ also passes under transformation into the multiplier s and conversely. Therefore, since the higher order impulses correspond to higher order derivatives, these cannot exist either for a passive network.

To produce a general means of solving the integral equation set represented by equation 15, it is proposed that

the integrals be evaluated numerically by some approximating technique such as that of Simpson. Following this, an iterative sequence is applied to extract the solutions for the currents i(t).

To evaluate the integrals numerically, it is assumed that the continuous functions of time appearing in the integrands may be adequately approximated by a sequence of rectangular pulses. Each pulse is of time duration Δt and of amplitude equal to that of the function evaluated at the central time of this time increment.

For a continuous function f(t), for $0 \leqslant t$,

$$f(t) \doteq f(0)\left[u_0(t) - u_0(t - \frac{\Delta t}{2})\right] + \sum_{g=1} f(g\Delta t)\left[u_0(t - \{g-\tfrac{1}{2}\}\Delta t) - u_0(t - \{g+\tfrac{1}{2}\}\Delta t)\right] . \tag{32}$$

Observe that the first interval is only half that of the remaining increments in view of the lower bound set on time. The product of two such functions approximated for the same time increment is defined by

$$f(t)h(t) \doteq f(0)h(0)\left[u_0(t) - u_0(t - \frac{\Delta t}{2})\right] + \sum_{g=1} f(g\Delta t)h(g\Delta t)\left[u_0(t - \{g-\tfrac{1}{2}\}\Delta t) - u_0(t - \{g+\tfrac{1}{2}\}\Delta t)\right] . \tag{33}$$

The definite integral of f(t) over an integral multiple of the time increment, $\tau = G\Delta t$, is then

$$\int_0^{\tau} f(t)dt \doteq f(0)\,\frac{\Delta t}{2} + \Delta t \sum_{g=1}^{G-1} f(g\Delta t) + f(\tau)\,\frac{\Delta t}{2}\ , \qquad (34)$$

the last as well as the first time increment being $\frac{\Delta t}{2}$ by the above definitions.

In addition to the provisions made for approximating continuous functions, special consideration must be given to the impulsive terms possibly occurring in the admittance functions and pseudo-driving voltages. To simplify the form of the approximation to equation 15, it is assumed that unit doublet terms have been eliminated, as previously discussed. Since the unit impulse does not lend itself to approximation as a series of time delayed rectangular pulses, terms in product with impulses will be treated separately. By definition, the unit impulse has the property of enclosing unit area and is effective at some time t_e for an infinitesimal time duration. Thus in product with some function f(t), defined at time t_e,

$$u_1(t - t_e)f(t) = f(t_e)u_1(t - t_e)\ . \qquad (35)$$

The result is a unit impulse of area equal to $f(t_e)$. Further, the definite integral of a unit impulse is defined as

$$\int_{t_1 \leqslant t_e}^{t_2 \geqslant t_e} u_1(t - t_e)dt \triangleq u_0(t - t_e)\ . \qquad (36)$$

The result is a unit step delayed t_e seconds in time. A

multiplicative factor f(t) in the integrand carries through by equation 35 as the constant multiplier $f(t_e)$.

With the tools developed in the preceding paragraphs, the approximating form of the representative integral equation 15 will be formed. Equation 15 is repeated in expanded form as

$$i_j(t) = \sum_{p=1}^{3} \int_0^t P_{pj}(t - \lambda) e_p(\lambda) d\lambda - \sum_{p=1}^{3} \int_0^t P_{pj}(t - \lambda) b_p(\lambda) d\lambda - \sum_{p=1}^{3} \int_0^t P_{pj}(t - \lambda) f_p(i; \lambda) d\lambda \quad . \tag{37}$$

In order to partition the general admittance function so that the unit impulse term appears separately, define

$$P_{pj}(t) \triangleq B_{1_{pj}} u_1(t) + P'_{pj}(t) \quad , \tag{38}$$

thus $P'_{pj}(t)$ is continuous for $0 \leq t$.

The expression of Figure 6 becomes the desired approximation to equation 37, and represents but one of the three similar equations for solution of the sample network of Figure 2 at time $\tau = G\Delta t$. The generalization to a network containing n independent loops is accomplished by setting the upper limit equal to n for the summations on p and j.

The computation to determine the $i(G\Delta t)$ proceeds sequentially through the time increments. For the time

$$
\begin{aligned}
i_j(\tau) &= i_j(G\Delta t) \\
&\doteq \sum_{p=1}^{3}\Bigg\{ e_p(0)P'_{pj}(\tau)\,\frac{\Delta t}{2} + \Delta t \sum_{g=1}^{G-1} e_p(g\Delta t)P'_{pj}(\tau - g\Delta t) \\
&\qquad + e_p(\tau)P'_{pj}(0)\,\frac{\Delta t}{2} + e_p(\tau)B_{1_{pj}} \\
&\qquad - \Big[- L_{pp}i_p(0) + \sum_{\substack{j=1 \\ j\neq p}}^{3} L_{pj}i_j(0) \Big] P_{pj}(\tau) \\
&\qquad - \Big[C_{pp}^{-1}q_p(0) - \sum_{\substack{j=1 \\ j\neq p}}^{3} C_{pj}^{-1}q_j(0) \Big] \Big[P'_{pj}(0)\tfrac{\Delta t}{2} + \Delta t \sum_{g=1}^{G-1} P'_{pj}(g\Delta t) + P'_{pj}(\tau)\tfrac{\Delta t}{2} + B_{1_{pj}} \Big] \\
&\qquad - \Big[f_p(i;0)P'_{pj}(\tau)\,\frac{\Delta t}{2} + \Delta t \sum_{g=1}^{G-1} f_p(i;g\Delta t)P'_{pj}(\tau - g\Delta t) \Big] \\
&\qquad - f_p(i;\tau)\Big[P'_{pj}(0)\,\frac{\Delta t}{2} + B_{1_{pj}} \Big] \Bigg\},
\end{aligned}
$$

for $\tau \geq 0$.

Figure 6. Approximating form of the representative integral equation 37 for a third order network

$\tau = G\Delta t$, the $i(g\Delta t)$ are known for $0 \leq g \leq G-1$. Therefore the expression of Figure 6 reduces to an equation for $i_j(\tau)$ in terms of known functions of time, denoted by $X_j(\tau)$, and the nonlinear contributions to the currents at time τ. Then

$$i_j(\tau) = i_j(G\Delta t) \doteq X_j(\tau) - \sum_{p=1}^{3} f_p(i;\tau) \left[P'_{pj}(0) \frac{\Delta t}{2} + B_{1_{pj}} \right] \quad (39)$$

becomes the representative expression to be iterated for the $i_j(\tau)$, for $j = 1,2,3$. To begin the solution sequence at $\tau = 1\Delta t$, the initial conditions in the linear elements are assumed given, thus the solution may proceed for the $i_j(\Delta t)$ in terms of these values at $g\Delta t = 0$. A discussion of the particular iterative scheme to be employed will be postponed until the next chapter.

This method of analysis may be extended to the treatment of active networks. For example, assume that $e_3(t)$ of Figure 2 is the output voltage of an amplifier with amplification factor μ. If the voltage at the grid of the amplifier is a fraction k of the voltage $R_2 i_2(t)$, then

$$e_3(t) = -\mu k R_2 i_2(t) \ . \quad (40)$$

The negative sign describes the plate to grid phase relationship of signals. If it is known that the voltage at the grid, $kR_2 i_2(t)$, will never exceed the limits of linear operation of the tube, then the driving voltage of equation 40 may be transposed as a voltage drop in equation 6. The

linear impedance operator z_{32} of equation 6 then becomes

$$z_{32} = L_{32} \frac{d}{dt} + R_{32} - \mu k R_2 + C_{32}^{-1} \int^t dt \qquad (41)$$

If the assumption that the linear relation 40 applies for the entire range of $i_2(t)$ is not valid, either of two courses may be followed. The first is to retain the definition of $e_3(t)$ as a driving voltage without influence on the linear impedance operator. The second course is to modify z_{32} as in equation 41, and define a driving voltage $\bar{e}_3(t)$ such that

$$\bar{e}_3(t) \triangleq e_3(t) + \mu k R_2 i_2(t) \qquad (42)$$

for the extended range of $i_2(t)$.

The occurrence of third and higher order impulses in the admittance functions of an active network cannot be definitely denied as in the case of passive networks. Therefore, the general definitions of these and their properties have been retained, although the specific treatment of these in the final numerical analysis is not included.

The ability to express nonlinear characteristics in the time domain without the explicit knowledge of their transforms permits considerable freedom in detailing element response characteristics observed experimentally. However, when the characteristic response is transposed as a pseudo-driving function, care must be taken in order that the

determinant of $[Z_{ij}(s)]$ does not become identically zero. In the limiting case where all elements are considered to possess nonlinear characteristics, this difficulty will arise, but may be circumvented by redefining the nonlinearities so that a finite linear element is present in each of the loops of the network.

There exists a practical upper limit on the span of time $\tau = G\Delta t$ for which a given computer can reasonably handle the volume of data required in Figure 6. This maximum time span will be designated as $\tau_u = G_u \Delta t$. The solutions for the interval $0 \leq t \leq \tau_u$ may be extended into the following time span $\tau_u \leq t \leq 2\tau_u$ with the real time τ_u considered as the new time origin. For the new span, the $e'_p(t)$ assume values starting at real time τ_u. The admittance functions remain unchanged since their form is based on the homogeneous statement of the linear portion of the set of integrodifferential equations for the network. Thus these are dependent only upon a virtual time origin set for the initial conditions.

The continued extension of the solutions by this means may in many instances be expected to yield an indication of the steady state responses. The general reliability of repeated extensions is limited by the accumulating error in the approximating forms of the set of integral equations. The influence of these errors and the dependency of the overall accuracy upon the selection of the appropriate time

increment are demonstrated and discussed in the chapters dealing with the application of this analysis method to some actual networks.

THE ITERATIVE SOLUTION OF THE SET OF INTEGRAL EQUATIONS

The solutions $i(\tau)$ are obtained by an iteration of the set of equations represented by equation 39. This equation is repeated for the case of n variables as

$$i_j(\tau) \doteq X_j(\tau) - \sum_{p=1}^{n} f_p(i;\tau) \left[P'_{pj}(0) \frac{\Delta t}{2} + B_{1_{pj}} \right]. \qquad (43)$$

The method of iteration to be used is outlined in equation 44. The superscript K = 0,1,2,... numbers the iterated results $i^{(K)}(\tau)$ and the solution estimates $\bar{i}^{(K)}(\tau)$ in the order in which they are formed.

$$\bar{i}_j^{(0)}(\tau) \triangleq \bar{i}_j^{(1)}(\tau)/\pi \ ,$$

$$\bar{i}_j^{(1)}(\tau) \triangleq X_j(\tau) \ ,$$

$$i_j^{(2)}(\tau) \triangleq X_j(\tau) - \sum_{p=1}^{n} f_p(\bar{i}^{(1)};\tau) \left[P'_{pj}(0) \frac{\Delta t}{2} + B_{1_{pj}} \right] ,$$

$\bar{i}_j^{(2)}(\tau)$ is derived from Figure 7 in terms of $i_j^{(2)}(\tau)$, (44)

$$\vdots$$

$$i_j^{(K+1)}(\tau) \triangleq X_j(\tau) - \sum_{p=1}^{n} f_p(\bar{i}^{(K)};\tau) \left[P'_{pj}(0) \frac{\Delta t}{2} + B_{1_{pj}} \right] ,$$

$\bar{i}^{(K+1)}(\tau)$ is derived from Figure 7 in terms of $i_j^{(K+1)}(\tau)$.

The solutions $i(\tau)$ follow from the sequence of estimates as

$$i(\tau) \doteq \lim_{K \to \infty} \left\{ \bar{i}^{(K)}(\tau) \right\} , \qquad (45)$$

if this limit exists. In practice, the iteration proceeds

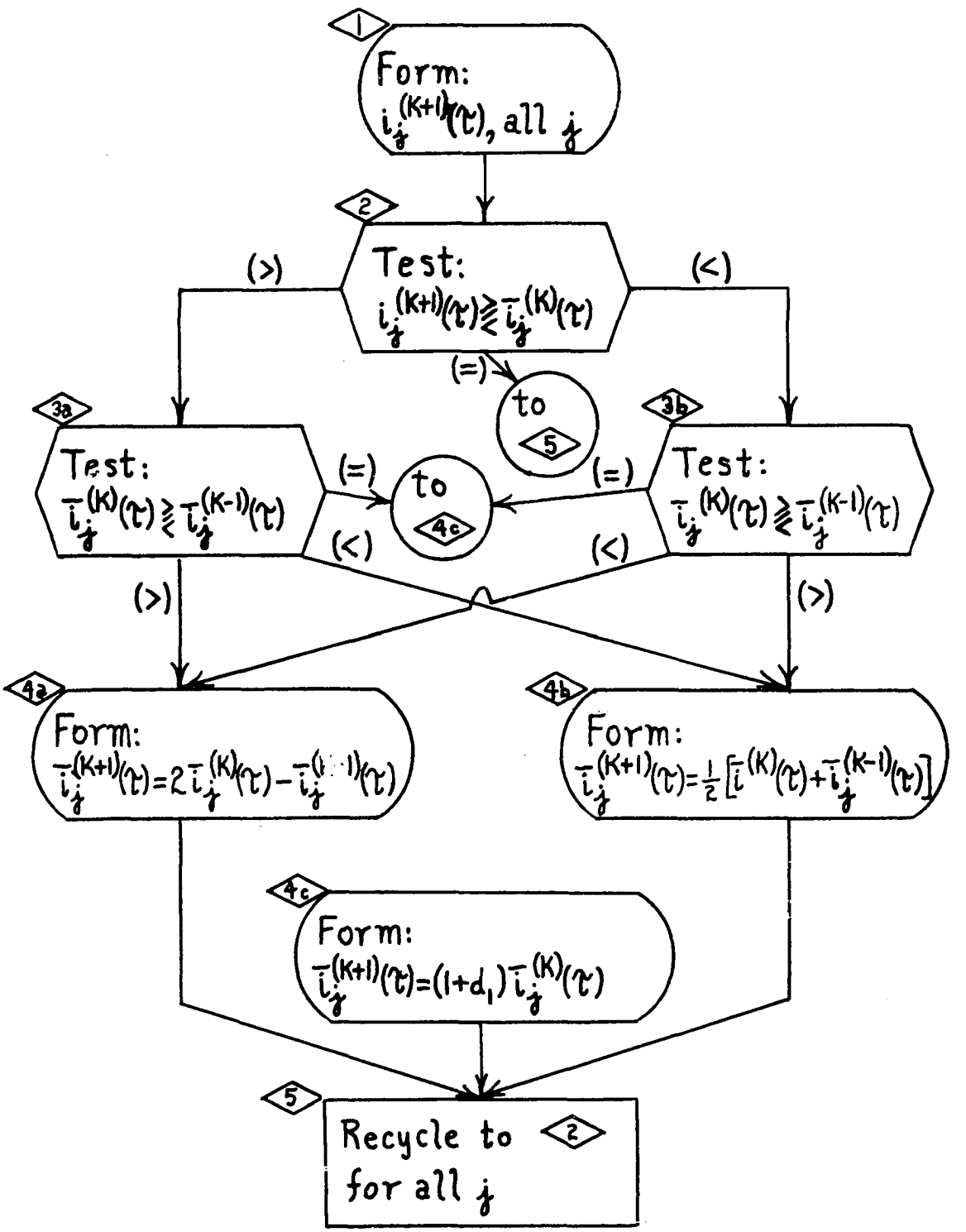

Figure 7. Logic schedule used in the interpretation of iterated results

until two successive estimates satisfy the inequality

$$\left| \frac{\bar{i}_j^{(K+1)}(\tau) - \bar{i}_j^{(K)}(\tau)}{\bar{i}_j^{(K)}(\tau)} \right| \leq d_2, \text{ for all } j \ . \qquad (46)$$

The constant d_2 is preset to specify the number of significant figures of convergence desired.

This proposed scheme of iteration is most readily discussed by contrasting it with the straightforward iterative method of equation 47.

$$\begin{aligned}
&\bar{i}_j^{(1)}(\tau) \triangleq X_j(\tau) \ , \\
&\bar{i}_j^{(2)}(\tau) \triangleq X_j(\tau) - \sum_{p=1}^{n} f_p(\bar{i}^{(1)};\tau) \left[P'_{pj}(0) \frac{\Delta t}{2} + B_{1_{pj}} \right] , \qquad (47) \\
&\quad \vdots \\
&\bar{i}_j^{(K+1)}(\tau) \triangleq X_j(\tau) - \sum_{p=1}^{n} f_p(\bar{i}^{(K)};\tau) \left[P'_{pj}(0) \frac{\Delta t}{2} + B_{1_{pj}} \right] \ .
\end{aligned}$$

Here the successive solution estimates are obtained directly from the iterated equation form. The basic difference between equations 44 and 47 is contained in the steps 4a, 4b and 4c of the logic schedule of Figure 7. In these steps, the estimate $\bar{i}_j^{(K+1)}(\tau)$ is formed by adjusting the estimate $\bar{i}_j^{(K)}(\tau)$ by a factor unrelated in magnitude to that of the iterated result $i_j^{(K+1)}(\tau)$. The value of this iterated result serves only to determine which of the steps 4 defines the appropriate adjustment. The magnitude of the

adjustment factor is defined initially as $\bar{i}_j^{(1)}(\tau)\left[1 - 1/\pi\right]$. The choice of $\pi = 3.141...$ as the constant relating $\bar{i}_j^{(0)}(\tau)$ and $\bar{i}_j^{(1)}(\tau)$ is arbitrary.

In the sequence of solution estimates formed by equation 44, each time that step 4b of Figure 7 is selected, the magnitude of the adjustment factor is halved. The implication is that the estimates $\bar{i}_j^{(K)}(\tau)$, $\bar{i}_j^{(K-1)}(\tau)$ have bracketed the actual solution. When step 4a is selected, no change is made in the magnitude of the adjustment factor. This implies that the estimates $\bar{i}_j^{(K)}(\tau)$, $\bar{i}_j^{(K-1)}(\tau)$ are both either greater or less than the actual solution, the estimate $\bar{i}_j^{(K)}(\tau)$ being nearest to the solution. Step 4c is included as an escape in the event of the false convergence of two successive solution estimates for the j^{th} current. When several currents are sought simultaneously, this may occur before all of the solution sequences have converged. This situation produces an equality exit from the steps 3 in the succeeding iteration for the j^{th} current. Since the original adjustment factor has now vanished, some other increment must be assumed to avoid the premature termination of the sequence of estimates. The method of step 4c disrupts the original sequence, but permits the continuation of the process through some parallel sequence of estimates. The positive fraction d_1 used for this purpose must be greater than the convergence factor d_2 previously described.

If the straightforward iteration is to converge, the equation implicitly defining the dependent variable must be iterated for the term of highest algebraic order in that variable. Therefore, the form of equation 47 implies that $f_p(i;\tau)$ is of algebraic order less than one in i_j if a convergent sequence is to result. The convergence of the iterative method of equation 44 is not dependent on the algebraic order of the variable i_j in the $f_p(i;\tau)$. This is illustrated for a simple network by applying both methods of iteration.

Assume a series combination of a linear resistance r_1 of 1 ohm, a nonlinear resistance with a characteristic

$$v_{NLR} = (\text{sgn } i)|i|^2 , \tag{48}$$

and a voltage source $e(t) = -3.75\, u_o(t)$. The mesh equation for this network is

$$e(t) = r_1 i(t) + [\text{sgn } i(t)]\ |i(t)|^2 . \tag{49}$$

The solution for the current at time $\tau = G\Delta t$ is, in the form of equation 43,

$$\begin{aligned} i(\tau) &= r_1^{-1} e(\tau) - [r_1^{-1} \text{ sgn } i(\tau)]\ |i(\tau)|^2 \\ &= -3.75 - [\text{sgn } i(\tau)]\ |i(\tau)|^2 . \end{aligned} \tag{50}$$

By inspection, $i(\tau) = -1.5$ amps is a solution to this equation.

The iterative method of equation 47 produces the following current estimates.

$$\begin{aligned}
\bar{i}^{(1)}(\tau) &= -3.75 , \\
\bar{i}^{(2)}(\tau) &= -3.75 + (3.75)^2 = 10.31 , \\
\bar{i}^{(3)}(\tau) &= -3.75 - (10.31)^2 = -110.15 , \\
\bar{i}^{(4)}(\tau) &= -3.75 + (110.15)^2 = 12{,}130 .
\end{aligned} \tag{51}$$

This sequence of estimates diverges rapidly from the solution.

The iterative method of equation 44 produces the following sequence of current estimates.

$$\begin{aligned}
\bar{i}^{(0)}(\tau) &= \bar{i}^{(1)}(\tau)/\pi = -1.18 , \\
\bar{i}^{(1)}(\tau) &= -3.75 , \\
i^{(2)}(\tau) &= -3.75 + (3.75)^2 = 10.31 , \\
\bar{i}^{(2)}(\tau) &= \tfrac{1}{2}\left[\bar{i}^{(1)}(\tau) + \bar{i}^{(0)}(\tau)\right] = -2.47 , \\
i^{(3)}(\tau) &= -3.75 + (2.47)^2 = 2.35 , \\
\bar{i}^{(3)}(\tau) &= 2\,\bar{i}^{(2)}(\tau) - \bar{i}^{(1)}(\tau) = -1.19 , \\
i^{(4)}(\tau) &= -3.75 + (1.19)^2 = -2.33 , \\
\bar{i}^{(4)}(\tau) &= \tfrac{1}{2}\left[\bar{i}^{(3)}(\tau) + \bar{i}^{(2)}(\tau)\right] = -1.83 .
\end{aligned} \tag{52}$$

The sequence of $\bar{i}^{(K)}(\tau)$ is seen to converge on the desired solution in this case. If equation 50 is rewritten and iterated for the second term $|i(\tau)|^2$, both iterative methods

are convergent.

The G_u+1 converged current values for the time span $0 \leq \tau \leq \tau_u$ are the amplitude coefficients for the assumed series of rectangular pulses,

$$i_j(\tau) \doteq i_j(0)\left[u_0(\tau) - u_0(\tau - \frac{\Delta t}{2})\right] + \sum_{g=1}^{G_u-1} i_j(g\Delta t)\left[u_0(\tau - \{g - \tfrac{1}{2}\}\Delta t) - u_0(\tau - \{g + \tfrac{1}{2}\}\Delta t)\right] + i_j(G_u\Delta t)\left[u_0(\tau - \{G_u - \tfrac{1}{2}\}\Delta t) - u_0(\tau - G_u\Delta t)\right] . \quad (53)$$

The numerical errors in this approximate solution of the integral equation 37 are attributable to two causes. The first is inherent in the means of approximating the integrals of equation 37 to give the form of equation 39. The second is an accumulative error due to the dependence of each of the $i_j(G\Delta t)$ on the approximately determined past history for the set of $i(G\Delta t)$. This second source causes the error in the solution to increase with the time span considered for any given Δt. It is necessary to develop the solution for two or more values of the time increment Δt to determine the degree of error introduced from these sources in a practical application of the analysis method.

Although the author is not presently equipped to produce a formal convergence proof of the iterative method of equation 44, certain sufficient conditions on the integral equations

represented by equation 37 are presented from a text by Moulton (5, pp. 179-198). These conditions are imposed over a closed region R of the currents i and time λ.

1. The integrands are single valued functions of the i and λ.

2. The integrands are continuous functions of λ.

3. The integrands possess the Lipschitz property in the i, uniformly with respect to λ. In other words, for every pair of values for the i, say i' and i", and all λ in R, the following inequality must apply.

$$\left|f_p(i';\lambda)P_{pj}(t-\lambda) - f_p(i";\lambda)P_{pj}(t-\lambda)\right| \leq A\sum_{p=1}^{n}\left|i'_j - i"_j\right|, \quad (54)$$

where A is a finite constant independent of the i and λ.

The unit impulses which occur in the $P_{pj}(t)$ and linear initial condition terms appear to violate condition 2 above. On the basis of physical intuition, one may argue that these impulses occur due to simplifying assumptions made in characterizing the elements of the network. Thus these terms represent transient effects of extremely short effective duration. If this is an acceptable interpretation, then the impulse can be replaced by a continuous function of extremely short duration and a correspondingly large, but finite amplitude characteristic. The time integral of this continuous function is equal to the area of the impulse replaced.

This viewpoint is the basis for the separate treatment given to the impulses to form the approximations of equation 39.

ANALYSIS OF PASSIVE NETWORKS WITH ONE NONLINEAR ELEMENT

For the two examples of this chapter and that of the next, the same basic passive network will be considered. Its schematic form appears in Figure 8. In Appendix D the mesh analysis equations for this network and the resulting admittance transforms are developed in general terms.

The first case to be treated places in series with R_1 of Figure 8 a nonlinear resistance whose volt-ampere characteristic is approximated by

$$v_{NLR} = (\text{sgn } i)\ 95.6|i|^{0.3922} . \qquad (55)$$

The development of this form appears in Appendix C. For the purpose of avoiding a unit doublet in the admittance function, this element is subdivided into a linear component of resistance r_1, and a nonlinear component having the revised characteristic

$$v'_{NLR} = (\text{sgn } i)\left[95.6|i|^{0.3922} - r_1|i|\right] \triangleq f_1(i;t) . \qquad (56)$$

The circuit for analysis is represented by Figure 9 where the resistance $r_1 = 1250$ ohms is absorbed by R_1.

For this example $e_2(t)$ is zero for all time, but $e_1(t)$ is assumed to be a periodic square wave of period $T = 38.5$ milliseconds. A typical period of this function is represented by

$$e_1(t) = -12.0\left[u_0(t) - u_0(t - T/2)\right] . \qquad (57)$$

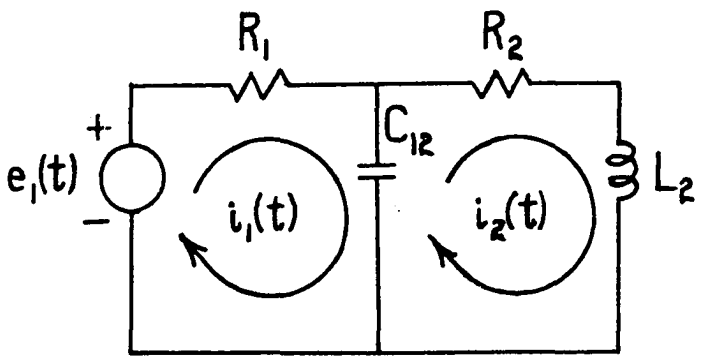

Figure 8. Basic passive network for analysis

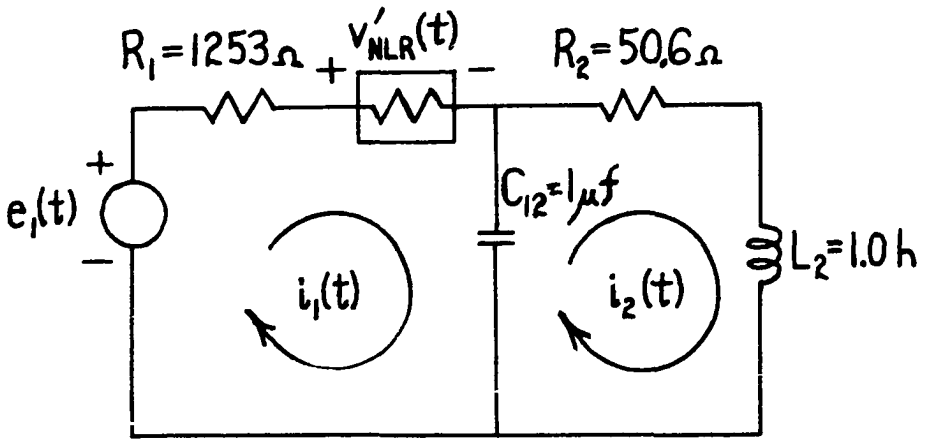

Figure 9. Network of Figure 8 with a nonlinear resistance added

It is observed that the last half period possesses zero voltage.

Upon substitution of the parameter values shown in Figure 9 in the admittance transforms of Appendix D, and the subsequent inverse transformation of these, there result for the admittance functions

$$P_{11}(t) = 0.798 \times 10^{-3}u_1(t) + 0.686e^{-424.3t}\sin(927t - 1.19),$$
$$P_{12}(t) = P_{21}(t) = 0.861e^{-424.3t}\sin(927t) , \qquad (58)$$
$$P_{22}(t) = 1.079e^{-424.3t}\sin(927t + 1.19) .$$

Their development appears in detail in Appendix E. The terms accounting for initial conditions, as developed in Appendices D and E, are

$$b_1(t) = 1 \times 10^6\left[q_1(0) - q_2(0)\right] u_0(t) \qquad (59)$$
$$b_2(t) = - 1.0\, i_2(0)u_1(t) + 1 \times 10^6\left[q_2(0)-q_1(0)\right] u_0(t).$$

All of the quantities required for the integral equation set are now defined for this example. Thus

$$i_1(t) = \int_0^t \left[e_1(\lambda) - b_1(\lambda) - f_1(i_1;\lambda)\right] P_{11}(t - \lambda)d\lambda$$
$$- \int_0^t b_2(\lambda)P_{21}(t - \lambda)d\lambda , \qquad (60)$$
$$i_2(t) = \int_0^t \left[e_1(\lambda) - b_1(\lambda) - f_1(i_1;\lambda)\right] P_{12}(t - \lambda)d$$
$$- \int_0^t b_2(\lambda)P_{22}(t - \lambda)d\lambda ,$$

for $t \geq 0$.

The time incremented approximations which the computer is programmed to operate on for time $\tau = G\Delta t$ appear in Figure 10. Although the initial condition currents and charges are to be taken as zero at the actual time origin, thus eliminating the $b_p(t)$ terms in the equation set 60, there remains the consideration of proceeding beyond the first time span τ_u. For such extensions the initial conditions will not in general be zero, thus these terms have been retained. In the expressions of Figure 10, the halving of the time increment at either end of the time span $G\Delta t$ has been omitted for the sake of brevity.

For this first example, a comparison of experimental and computed responses appears in Figures 11 and 12 for the currents $i_1(t)$ and $i_2(t)$ respectively. Figures 13 and 14 present the computed current responses $i_1(t)$ and $i_2(t)$ respectively, for three choices of the time increment Δt used in the computation. The responses corresponding to the finer increment of 0.1 milliseconds are those appearing with the experimental responses in Figures 11 and 12. This choice is based on the observation that the three solutions, ordered by decreasing time increment, appear to form a converging sequence. The basic points of comparison are the relative amplitudes and times of occurrence of adjacent crests of a given solution with those of a differently time incremented

$$
\begin{aligned}
i_1(\tau) \doteq & \sum_{g=0}^{G} e_1(g\Delta t)P'_{11}(\tau - g\Delta t)\Delta t + e_1(\tau)B_{1_{11}} \\
& - 10^6\left[q_1(0) - q_2(0)\right]\left\{B_{1_{11}} + \sum_{g=0}^{G} P'_{11}(g\Delta t)\Delta t\right\} - \sum_{g=0}^{G-1} f_1(i_1;g\Delta t)P'_{11}(\tau - g\Delta t)\Delta t \\
& + L_2 i_2(0)P_{21}(\tau) - 10^6\left[q_2(0) - q_1(0)\right] \sum_{g=0}^{G} P'_{21}(g\Delta t)\Delta t \\
& - f_1(i_1;\tau)\left[P'_{11}(0)\Delta t + B_{11}\right] , \\
i_2(\tau) \doteq & \sum_{g=0}^{G} e_1(g\Delta t)P'_{12}(\tau - g\Delta t)\Delta t \\
& - 10^6\left[q_1(0) - q_2(0)\right] \sum_{g=0}^{G} P'_{12}(g\Delta t)\Delta t - \sum_{g=0}^{G-1} f_1(i_1;g\Delta t)P'_{12}(\tau - g\Delta t)\Delta t \\
& + L_2 i_2(0)P_{22}(\tau) - 10^6\left[q_2(0) - q_1(0)\right] \sum_{g=0}^{G} P'_{22}(g\Delta t)\Delta t \\
& - f_1(i_1;\tau)P'_{22}(0)\Delta t ,
\end{aligned}
$$

for $0 \leq \tau$.

Figure 10. Approximating forms of equation 75 for digital solution

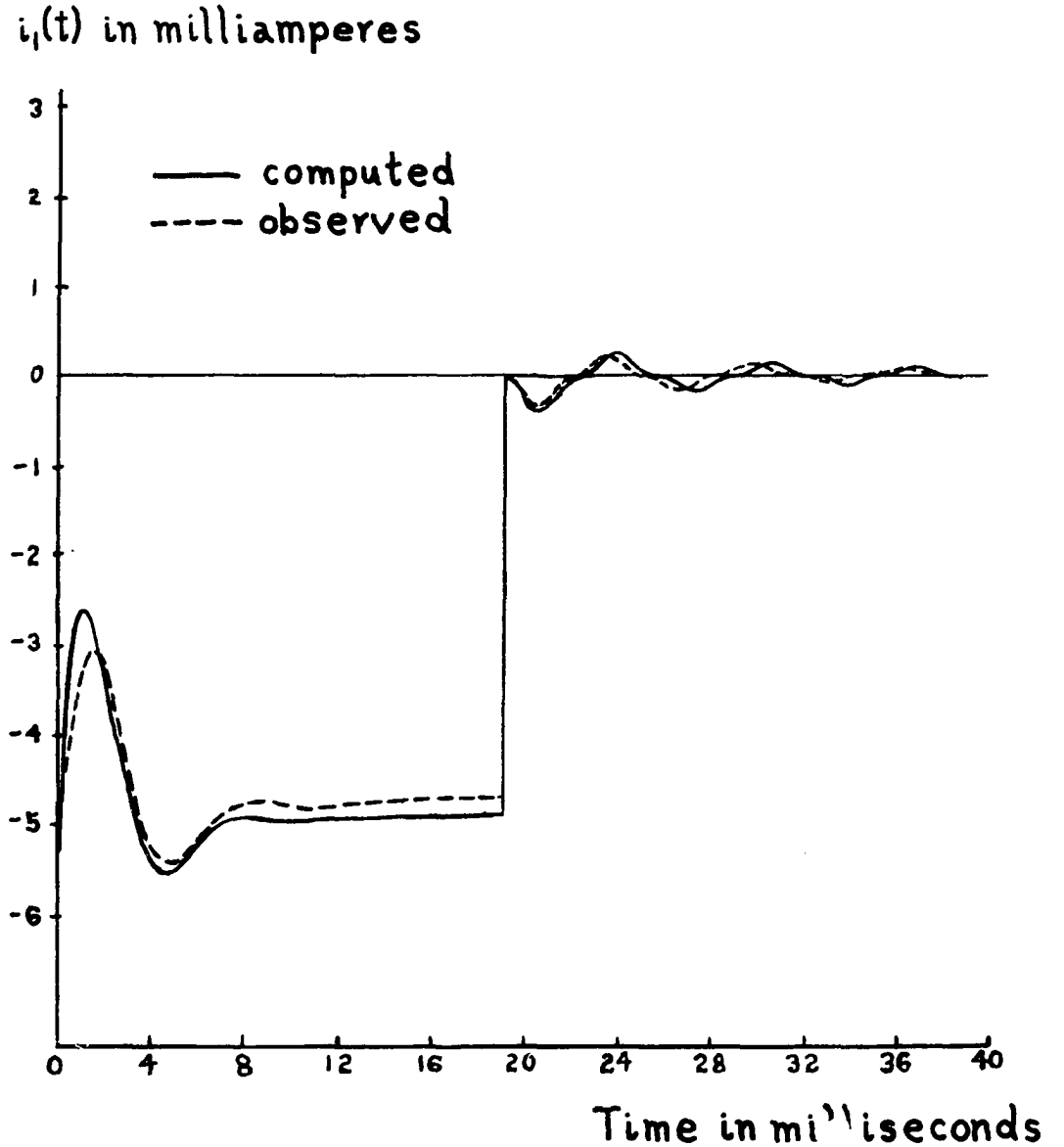

Figure 11. Comparison of observed and computed response $i_1(t)$ of Figure 9

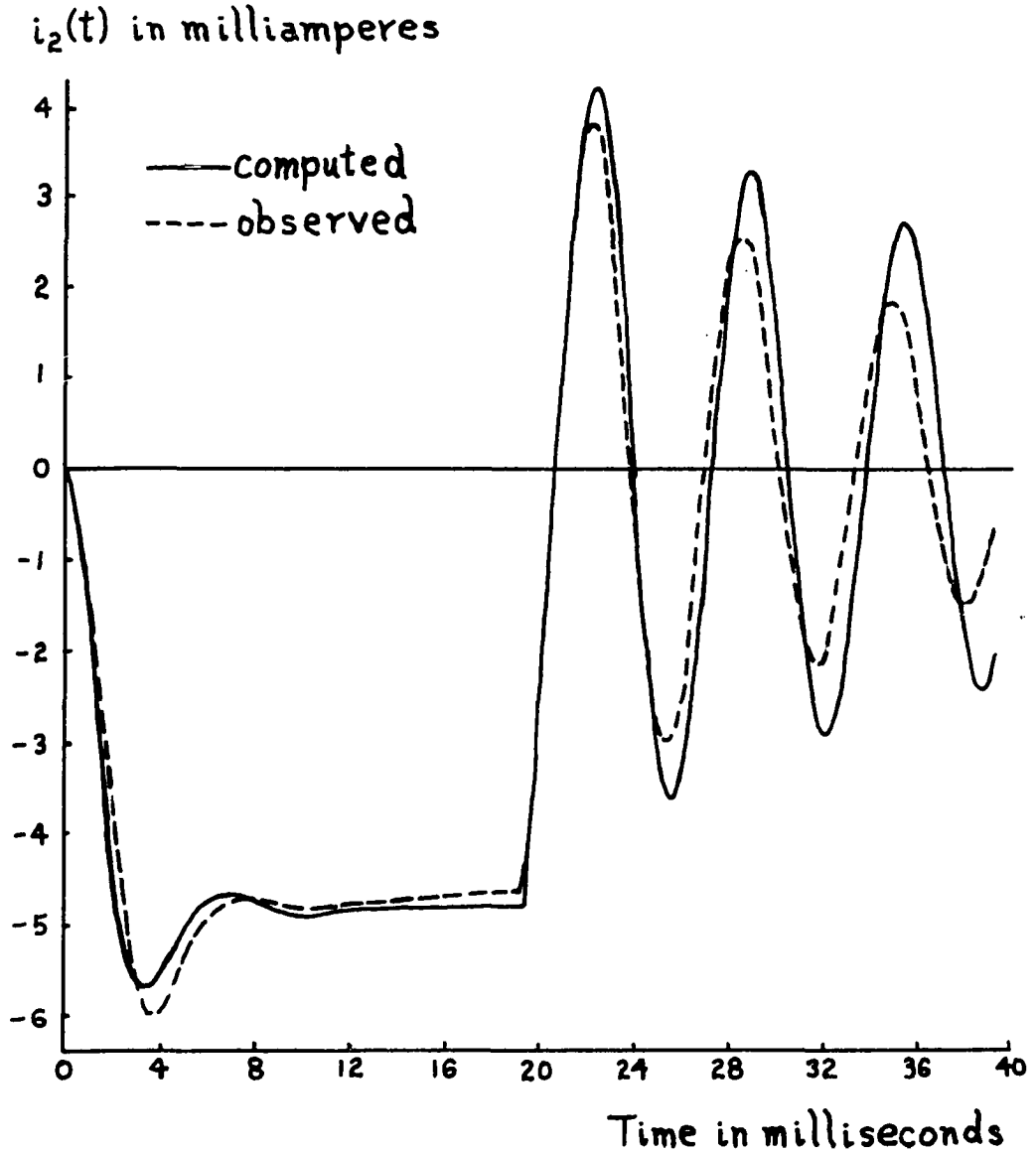

Figure 12. Comparison of observed and computed response $i_2(t)$ of Figure 9

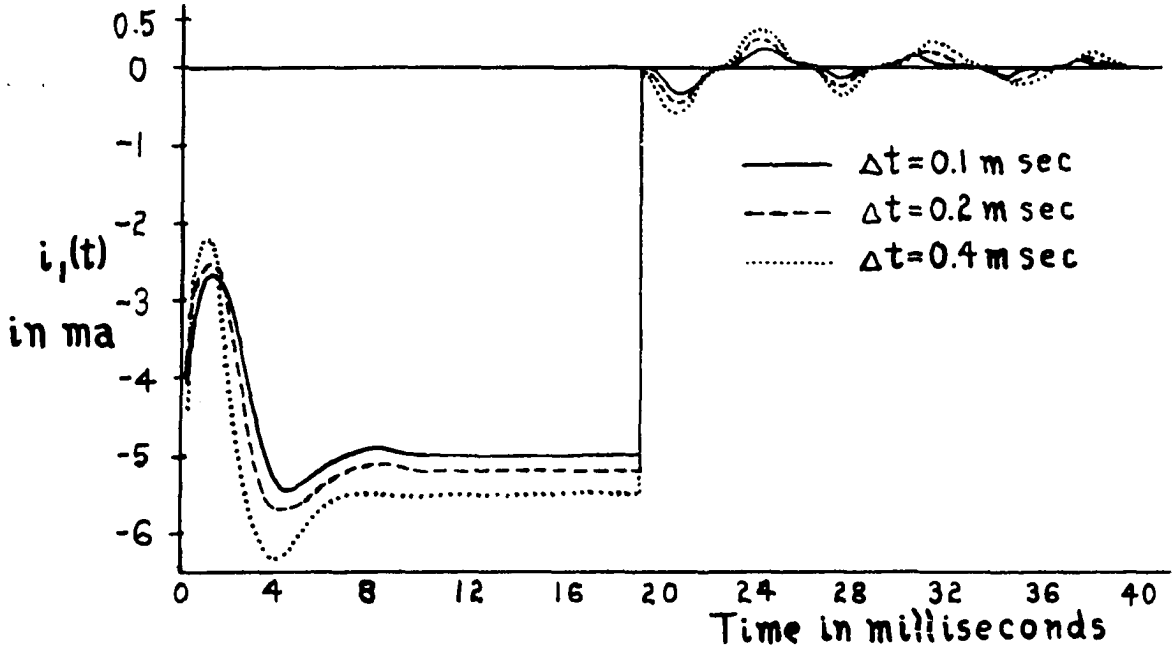

Figure 13. $i_1(t)$ of Figure 9 computed by varying Δt

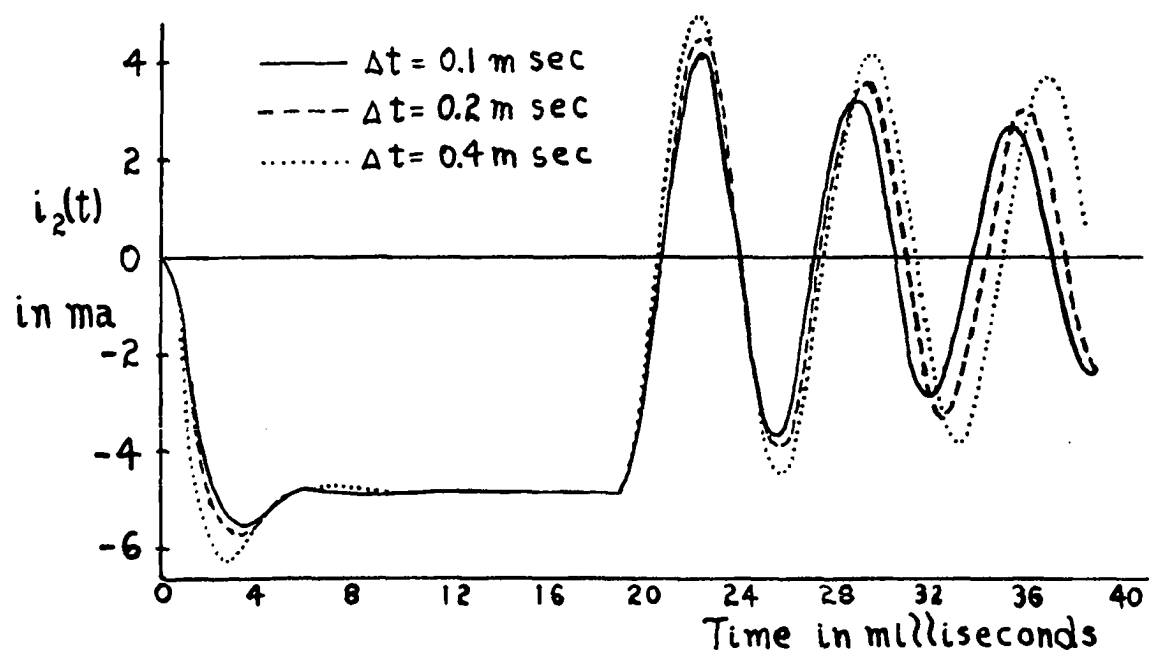

Figure 14. $i_2(t)$ of Figure 9 computed by varying Δt

solution. Some generalizations drawn from these comparisons are:

1. The initial surge of a given transient response will peak more prematurely in time for a coarser resolution of Δt.

2. Following the initial surge of a given transient response there exists a contraction in the fundamental period of the decaying response for a finer resolution of Δt.

3. The maxima and minima of the transient response decrease with a finer resolution of the Δt.

4. The decay time of the major exponential envelope associated with a given transient response decreases with a finer resolution of Δt.

These generalizations are all in accord with the discussion of the preceding chapter relative to the error introduced in the computation. There it was observed that an accumulative error exists in the converged solution estimate at a given time due not only to the approximate evaluation of the convolution integrals for this time, but due also to the same error in the past history values of the convolution products dependent on the responses sought. Recourse to a smaller time increment in the approximating functions is seen to improve the accuracy over a greater time span. The selection of an appropriate time increment without a foreknowledge of the actual response becomes a matter of establishing the sequence of solutions for decreasing time

increments. The comparison of successive computed responses indicates the degree of accuracy obtained.

A discussion of the deviation of the computed and experimental responses of Figures 11 and 12 must include the following.

1. Numerical approximation of the convolution integrals.

2. Inadequate definition of the nonlinear characteristic.

3. Inaccuracies in the experimental simulation.

The first of these causes has been discussed above. The definition of the nonlinear characteristic for this resistive element is seen from Figure 31 in Appendix B to be quite good over the range of values arising in this example. Therefore this should introduce little or no discrepancy in the responses observed and calculated. The inaccuracies in the simulation of this case appear primarily in the loading effect of the network on the power supply. This is evidenced in the upper curve of Figure 15 which represents the actual voltage output to the network. The effects of this loading have not been included in the computed current responses.

The network configuration, linear parameter values, and square wave frequency are so chosen as to produce a pronounced indication of the nonlinear effects in response to an excitation resembling that of a unit step. However, in

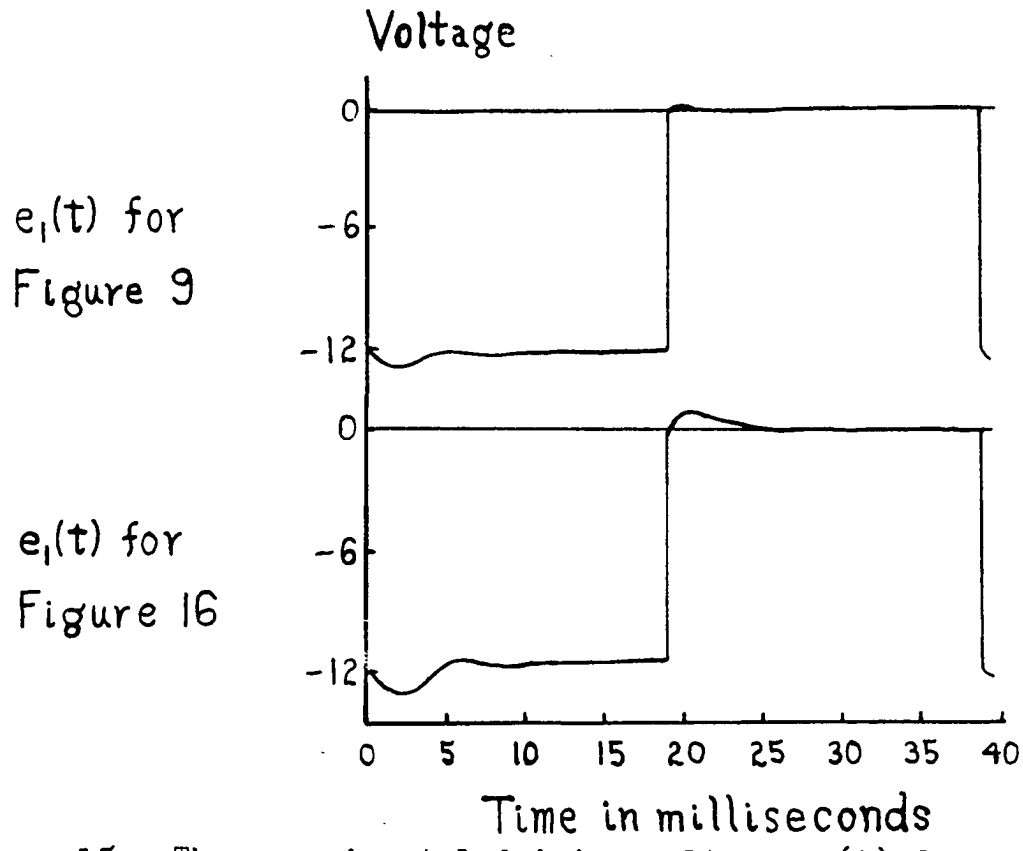

Figure 15. The experimental driving voltage $e_1(t)$ for Figures 9 and 16

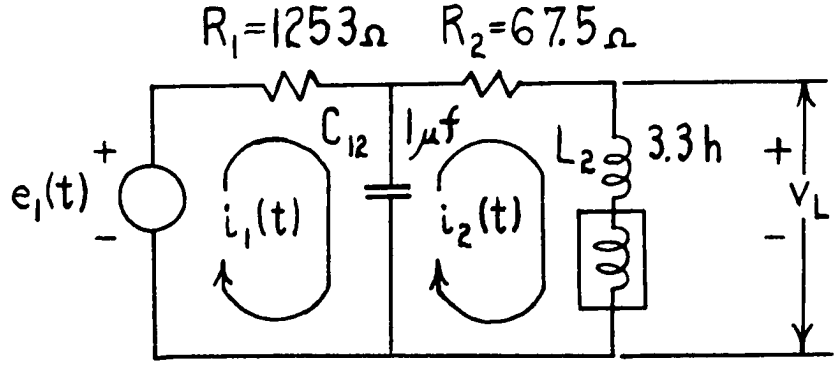

Figure 16. Network of Figure 8 with a nonlinear inductance added

order to achieve this, one accepts a widely varying level of input impedance to the network. This is particularly true in the use of the nonlinear resistance in series with the voltage source. The incremental resistance of this element varies from a few megohms at near zero current to values in the neighborhood of one kilohm at five or six milliamperes. The current response $i_1(t)$ penetrates the low resistance region rapidly in the first half cycle, thus producing the distortion in the actual voltage wave.

The overshoot of the voltage wave form in the first three of four milliseconds of the cycle produces excessive peaking in the current responses during this time. Undoubtedly this influences the remainder of the first half cycle response to a lesser degree since this is a function of its past history. It is felt, however, that the simulated response shown is adequate for the purpose of verifying the nature of the computed response. For the second half cycle the loading is much less and the correspondence of the comparisons of Figures 11 and 12 is much improved in this area.

A second variation on the basic network of Figure 8 restores R_1 as a linear resistance and gives L_2 a nonlinear characteristic. The circuit for analysis appears in Figure 16. The inductive effect is subdivided into a linear and non-linear series combination such that the voltage drop v_L

across the pair is

$$v_L = \frac{d\lambda(i_2;t)}{dt} \tag{61}$$

$$\triangleq \frac{d}{dt}\left[L_2 i_2(t) + \lambda'(i_2;t)\right]$$

$$\triangleq L_2 \frac{di_2(t)}{dt} + f_2(i_2;t) ,$$

where $\lambda(i_2;t)$ represents the magnetic flux as a function of the current $i_2(t)$. The segmented approximation to the observed mean magnetization curve of this element is developed in Appendix C as

$$\lambda_1 = 3.3i , \tag{62}$$

for $0 \leq |i| \leq 2.0 \times 10^{-3}$,

$$\lambda_2 = (\text{sgn } i)\left[-67.5|i|^2 + 2.398|i| + 1.973\times10^{-3}\right],$$

for $2.0 \times 10^{-3} \leq |i| \leq 10.0 \times 10^{-3}$,

$$\lambda_3 = (\text{sgn } i)\left\{\lambda_2(10.0\times10^{-3}) + 0.935\left[|i| - 10.0\times10^{-3}\right]\right\},$$

for $10.0 \times 10^{-3} \leq |i|$.

The $\lambda'(i_2;t)$ which appears in the intermediate form of equation 61 is formed by extracting the linear factor L_2 corresponding to the assumed maximum incremental inductance of the characteristic. Thus the nonlinear flux-current characteristic becomes

$$\lambda'_1 = 0 ,$$

for $0 \leq |i| \leq 2.0 \times 10^{-3}$, (63)

$$\lambda'_2 = (\text{sgn } i)\left[-67.5|i|^2 - 0.902|i| + 1.973 \times 10^{-3}\right],$$

for $2.0 \times 10^{-3} \leq |i| \leq 10.0 \times 10^{-3}$,

$$\lambda'_3 = (\text{sgn } i)\left\{\lambda'_2(10.0 \times 10^{-3}) + 0.935\left[|i| - 10.0 \times 10^{-3}\right]\right\},$$

for $10.0 \times 10^{-3} \leq |i|$.

Using the parameter values shown in Figure 16, the admittance functions for this network are

$$P_{11}(t) = 0.798 \times 10^{-3}u_1(t) + 0.900e^{-409.23t}\sin(389.75t - 0.788),$$

$$P_{12}(t) = P_{21}(t) = 0.620e^{-409.23t}\sin(389.75t) , \qquad (64)$$

$$P_{22}(t) = 0.428e^{-409.23t}\sin(389.75t + 0.788) .$$

These are developed in detail in Appendix F as also the linear initial condition terms as follow.

$$b_1(t) = 1 \times 10^6\left[q_1(0) - q_2(0)\right]u_0(t) , \qquad (65)$$

$$b_2(t) = -3.3i_2(0)u_1(t) + 10^6\left[q_2(0) - q_1(0)\right]u_0(t) .$$

Initial conditions at the real time origin are taken equal to zero and the driving voltage $e_1(t)$ is identical with that assumed in the first example. A typical period is represented by equation 57.

The solution set is now

$$i_1(t) = \int_0^t \left[e_1(\lambda) - b_1(\lambda)\right]P_{11}(t - \lambda)d\lambda - \int_0^t \left[b_2(\lambda) + f_2(i_2;\lambda)\right]P_{21}(t - \lambda)d\lambda , \qquad (66)$$

$$i_2(t) = \int_0^t \left[e_1(\lambda) - b_1(\lambda)\right] P_{12}(t - \lambda)d\lambda$$
$$- \int_0^t \left[b_2(\lambda) + f_2(i_2;\lambda)\right] P_{22}(t - \lambda)d\lambda \quad .$$

Attention is now drawn to the induced voltage $f_2(i_2;t)$ of equation 61, in particular to the determination of its value at time τ for use in the approximating forms for equation 66. The value of $\lambda'(i_2;\tau)$ is available in terms of the latest estimate for the current $i_2(\tau)$ from equation 63, but its derivative must be obtained empirically. In this analysis, the derivative required is approximated by

$$f_2(i_2;\tau) \doteq \frac{\lambda'(i_2;\tau) - \lambda'(i_2;\tau - \Delta t)}{\Delta t} \quad , \qquad (67)$$

although this value actually applies only at some intermediate time t in the interval $\tau - \Delta t \leq t \leq \tau$. The errors so incurred may be minimized by decreasing the time increment used and/or the use of difference tables formed from the flux function $\lambda'(i_2;t)$ for past time increments.

In Figures 17 and 18 are presented the experimental and computed responses for the currents $i_1(t)$ and $i_2(t)$ respectively. The computed response shown corresponds to the finest time increment used for this case, namely 0.1 milliseconds. Figures 19 and 20 compare the solutions obtained for three choices of the time increment. The generalizations drawn in a comparison of the computed responses for the first example appear to apply in this case also, with the

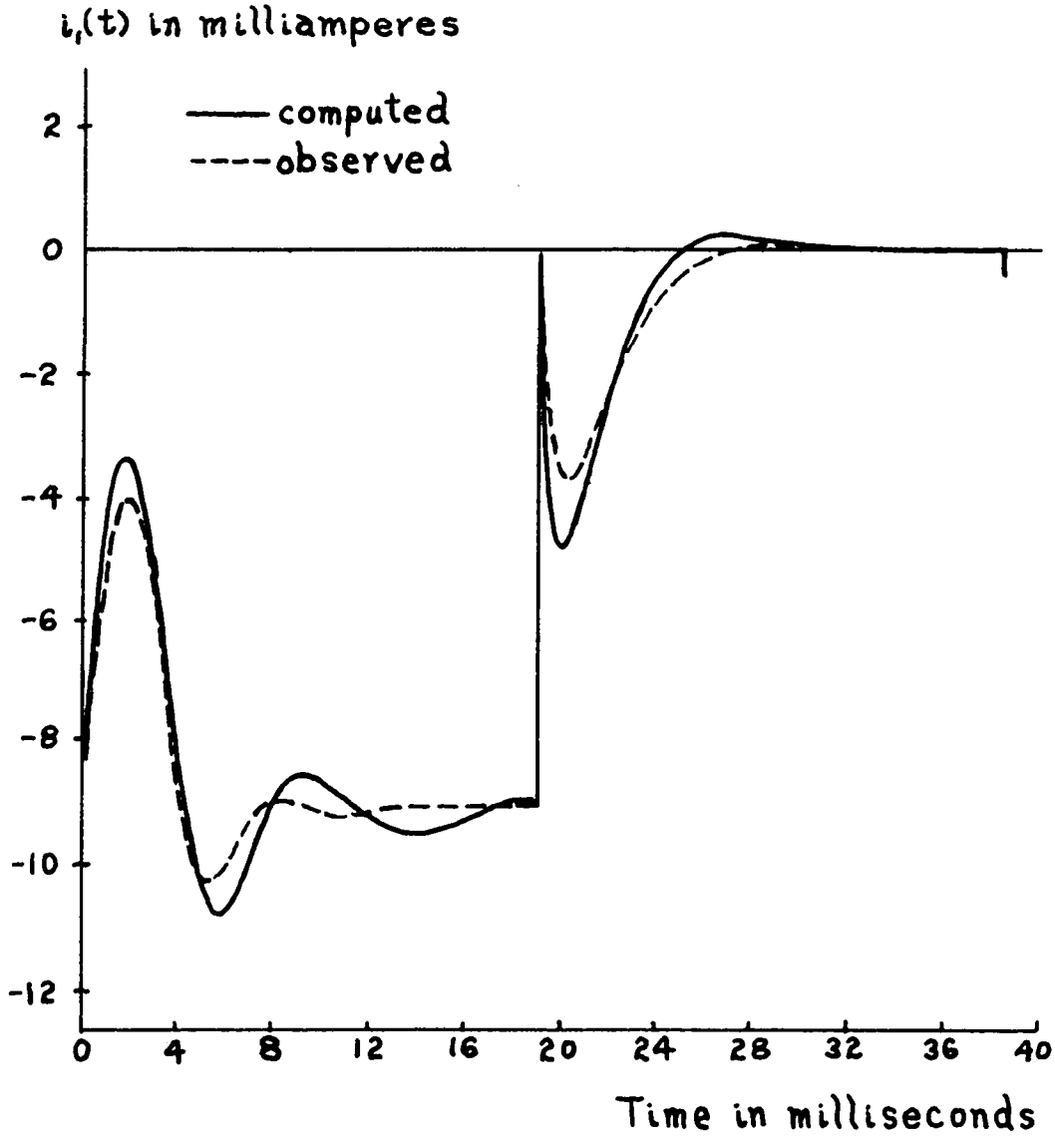

Figure 17. Comparison of observed and computed response $i_1(t)$ for Figure 16

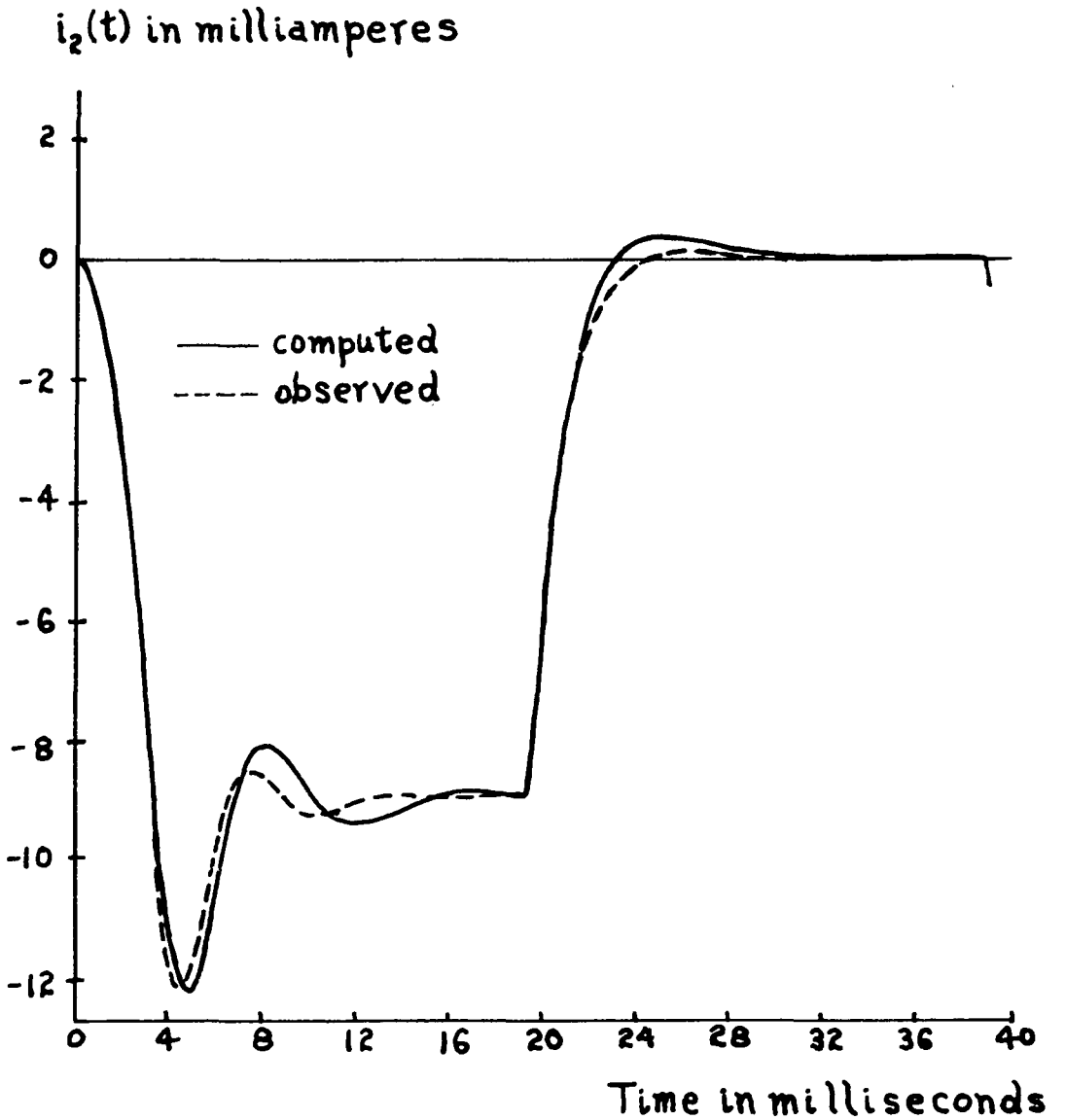

Figure 18. Comparison of observed and computed response $i_2(t)$ for Figure 16

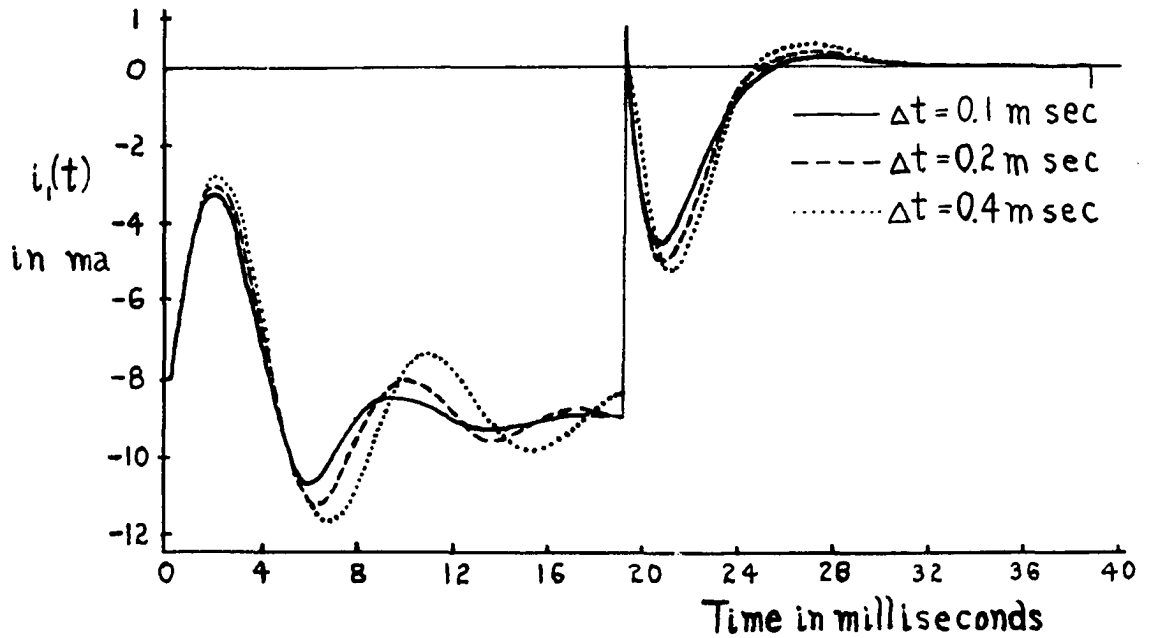

Figure 19. $i_1(t)$ of Figure 16 computed by varying Δt

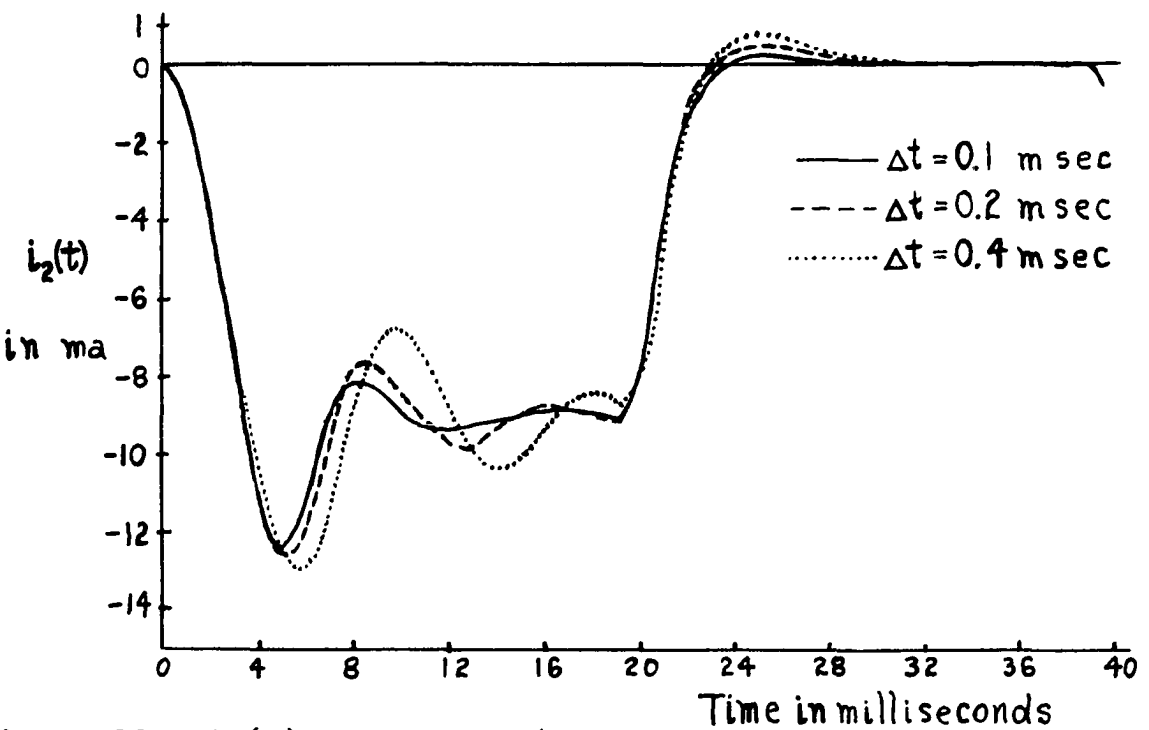

Figure 20. $i_2(t)$ of Figure 16 computed by varying Δt

exception of that concerning the premature peaking of the initial surge of the transient response. This exception is attributed to the error in evaluating the required derivatives, since this error effectively produces a time delay of the response in assuming any change in slope. This also accounts for the marked contraction of the fundamental period of the decaying response with decreasing values of the time increment.

The differences observed in the experimental and computed responses of Figures 17 and 18 will be discussed in terms of the three general causes introduced in the discussion of the first example. The error introduced due to numerical integration remains of a compounding nature, and is augmented by the additional error in the assigned time of occurrence of the derivatives, as in equation 67. The experimental simulation is inaccurate in this case also due to loading effects on the voltage source. This experimental voltage wave form appears in Figure 15. The low value of 1250 ohms assigned to the linear resistance R_1 is responsible for the distorted voltage wave form in both half cycles, but was necessary to produce the nonlinear effects pronouncedly. The loading effect on $e_1(t)$ is not included in the computations.

The errors introduced by the approximation of the hysteresis characteristics for the saturable transformer by

its mean magnetization curve are of potentially great significance. In the present example the decaying oscillations of the transient response are of sufficiently small amplitude to assume a negligible enclosed area within the hysteresis path followed. Thus the single valued characterization becomes practical. If, however, one attempts to analyze this network under sinusoidal excitation with an amplitude of several volts, a more elaborate description of the characteristic is probably required to obtain close agreement between theory and practice. This latter contention is based on an examination of the hysteresis family of Figure 32 in Appendix C for unbiased excitation, and that of Figure 33 for the biased condition. In either case, the significant areas encompassed by the large signal paths are observed. In particular, the current levels at which a marked change of slope occurs differ significantly for the paths of increasing and decreasing current.

ANALYSIS OF A PASSIVE NETWORK WITH TWO NONLINEAR ELEMENTS

The third example to be analyzed augments both R_1 and L_2 of the two mesh network of Figure 8 with the nonlinear elements considered separately in the preceding chapter. In Figure 22 is presented the revised network for analysis. The induced voltages v_{NLR} and v_L retain their definitions from equations 56 and 61 respectively. The square wave of voltage $e_1(t)$ of equation 57 is again applied, and the initial condition terms at the real time origin are set equal to zero.

The linear content of this system is identical with that of the second example of the preceding chapter, thus the linear admittance functions and initial condition terms remain unchanged from those developed in Appendix F, and recalled below.

$$
\begin{aligned}
P_{11}(t) &= 0.798 \times 10^{-3} u_1(t) + 0.900 e^{-409.23t} \sin(389.75t - 0.788), \\
P_{12}(t) &= P_{21}(t) = 0.620 e^{-409.23t} \sin(389.75t) , \\
P_{22}(t) &= 0.428 e^{-409.23t} \sin(389.75t + 0.788) , \\
b_1(t) &= 1 \times 10^{6} \left[q_1(0) - q_2(0) \right] u_0(t) , \\
b_2(t) &= -3.3 i_2(0) u_1(t) + 1 \times 10^{6} \left[q_2(0) - q_1(0) \right] u_0(t) .
\end{aligned}
\tag{68}
$$

The integral equation set for solution is now

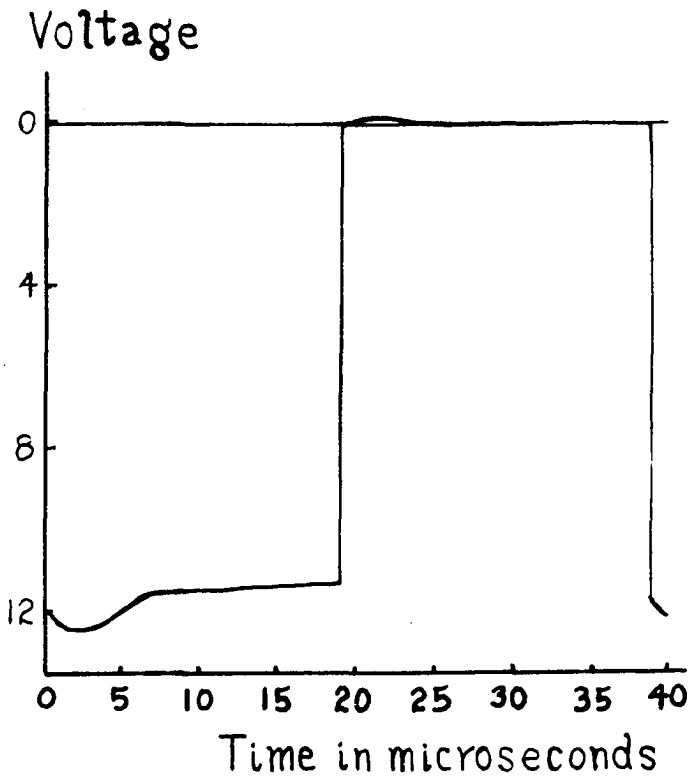

Figure 21. The experimental driving voltage $e_1(t)$ for Figure 22

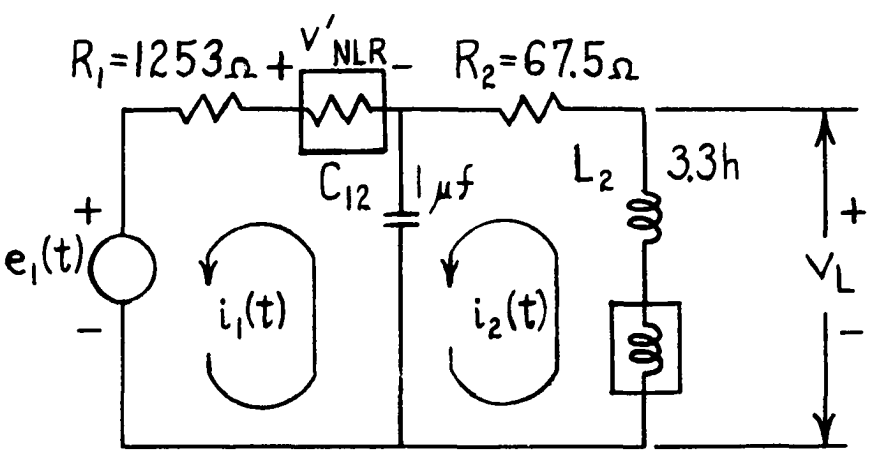

Figure 22. The network of Figure 8 with added nonlinear resistance and inductance

$$i_1(t) = \int_0^t \left[e_1(\lambda) - b_1(\lambda) - f_1(i_1;\lambda)\right] P_{11}(t-\lambda)d\lambda - \int_0^t \left[b_2(\lambda) + f_2(i_2;\lambda)\right] P_{21}(t-\lambda)d\lambda \quad , \tag{69}$$

$$i_2(t) = \int_0^t \left[e_1(\lambda) - b_1(\lambda) - f_1(i_1;\lambda)\right] P_{12}(t-\lambda)d\lambda - \int_0^t \left[b_2(\lambda) + f_2(i_2;\lambda)\right] P_{22}(t-\lambda)d\lambda \quad ,$$

for $t \geq 0$.

In Figures 23 and 24 are presented the comparisons of observed and computed responses for $i_1(t)$ and $i_2(t)$ respectively. The computed response corresponds to the use of a 0.1 millisecond time increment. This is the finest resolution of the three used in producing the sequence of current solutions which appear in Figures 25 and 26. The generalizations drawn in the last chapter appear again to apply, with the exception of that regarding the premature peaking of the initial transient surges. This exception, and the rapid contraction of the fundamental frequency of the decaying response with decreasing time increment are attributed to the delaying effect of the numerical evaluation of the time derivative required for $f_2(i_2;t)$. The degree of improvement observed by halving the time increment implies the need of a still finer resolution of the time increment to obtain the same degree of accuracy as was obtained in the first example. This is also demonstrated by the difference in amplitude of the observed and computed responses in the

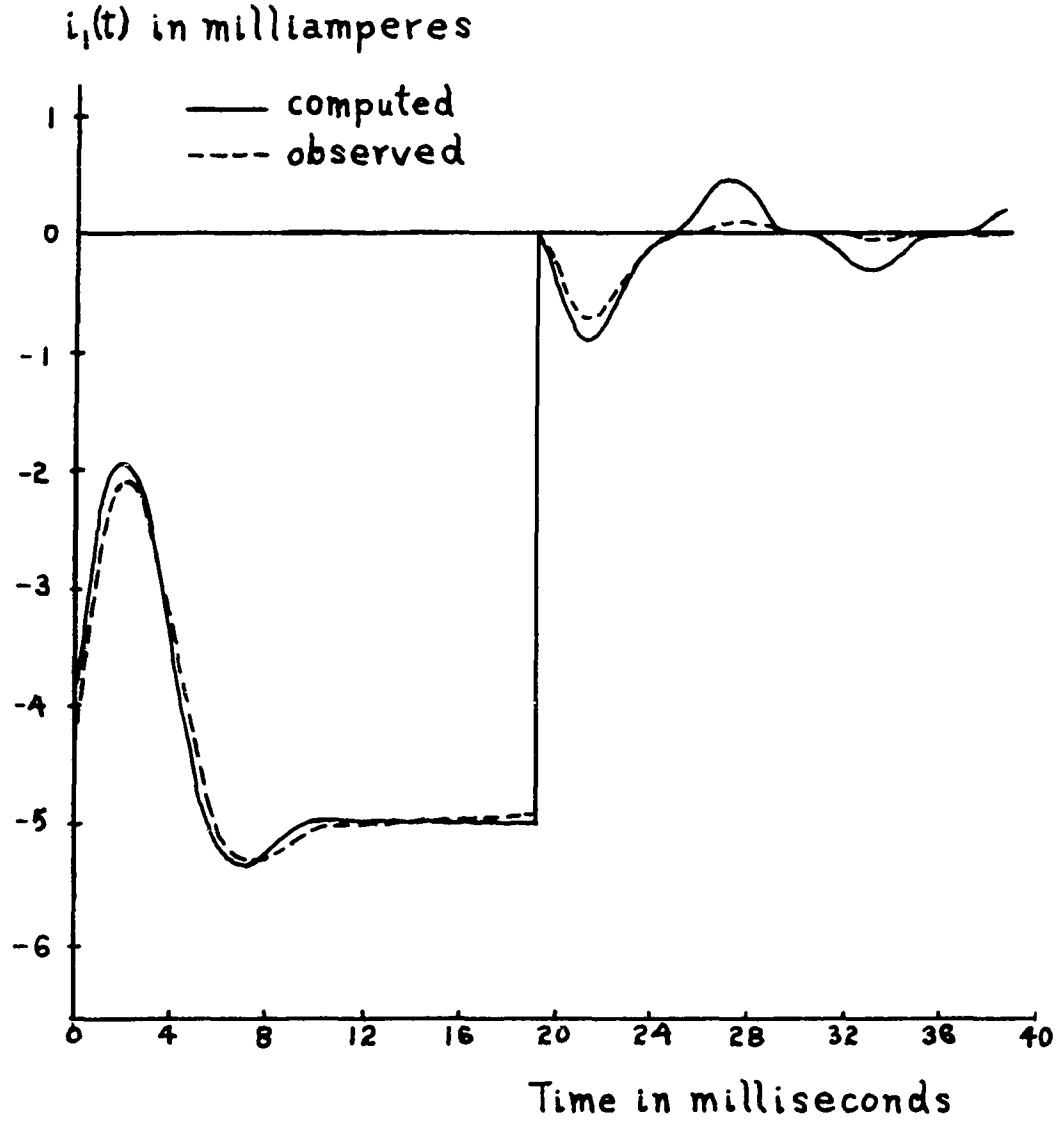

Figure 23. Comparison of observed and computed response $i_1(t)$ for Figure 22

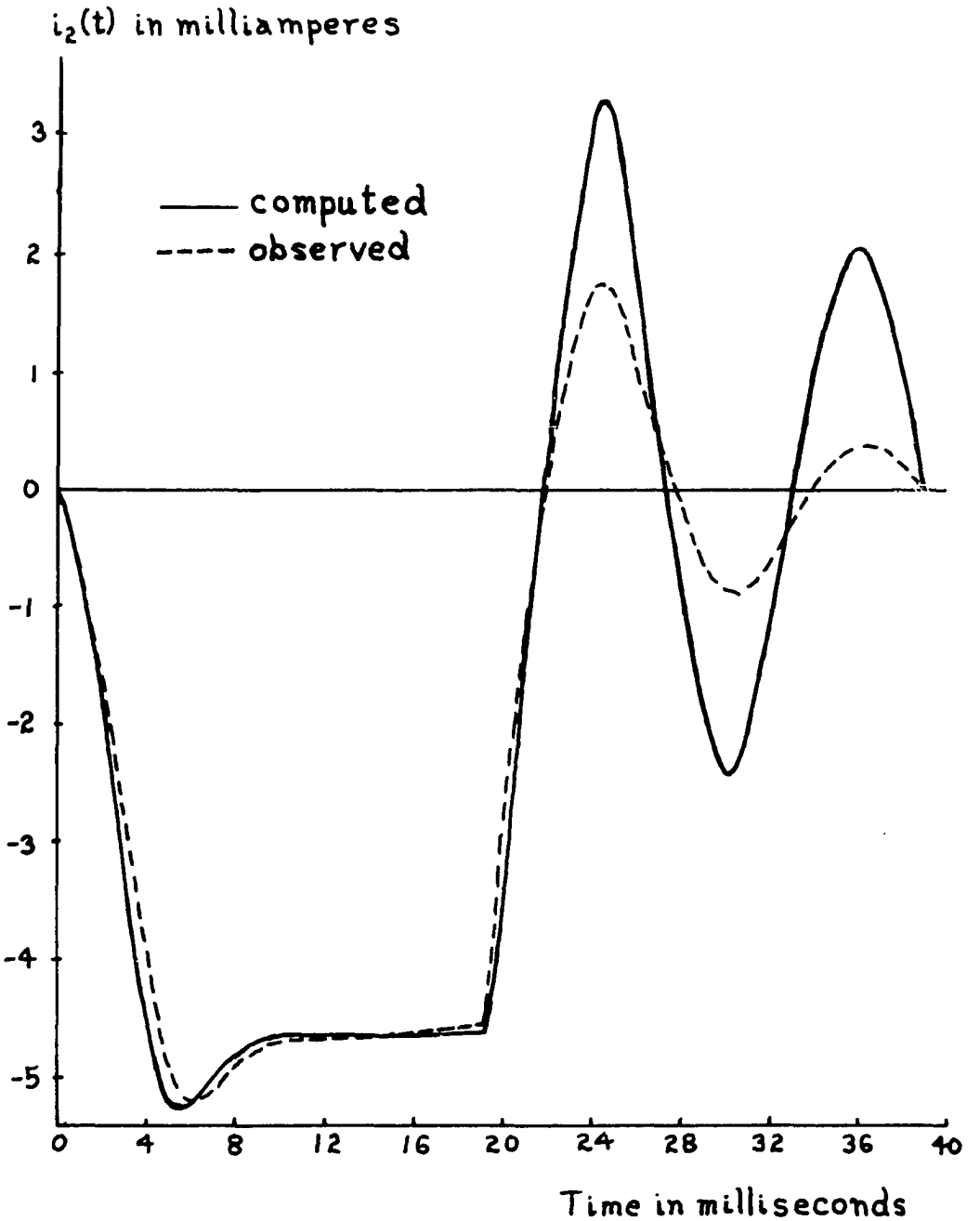

Figure 24. Comparison of observed and computed response $i_2(t)$ for Figure 22

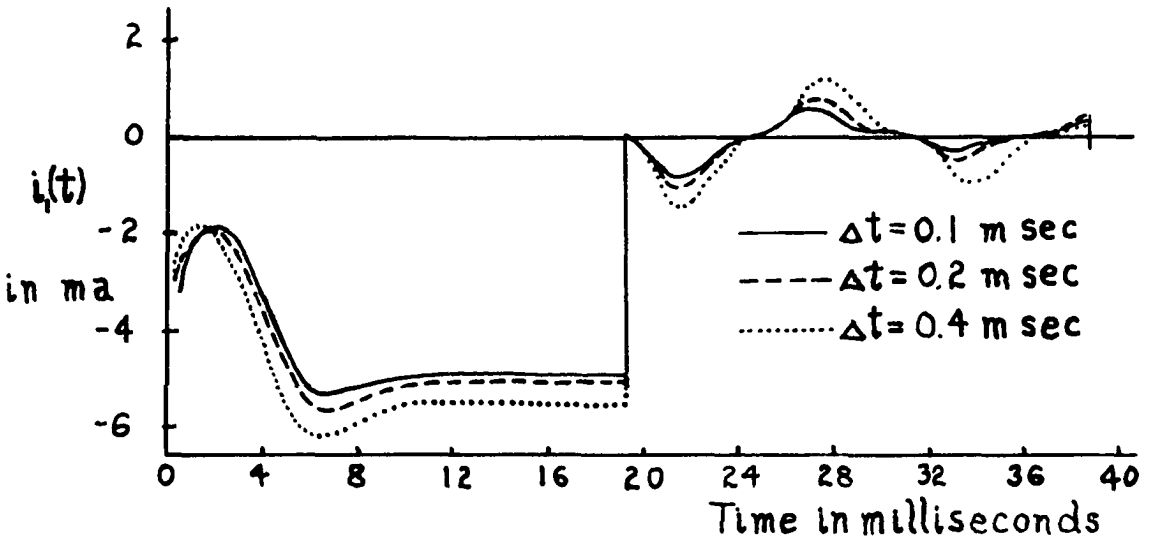

Figure 25. $i_1(t)$ of Figure 22 computed by varying Δt

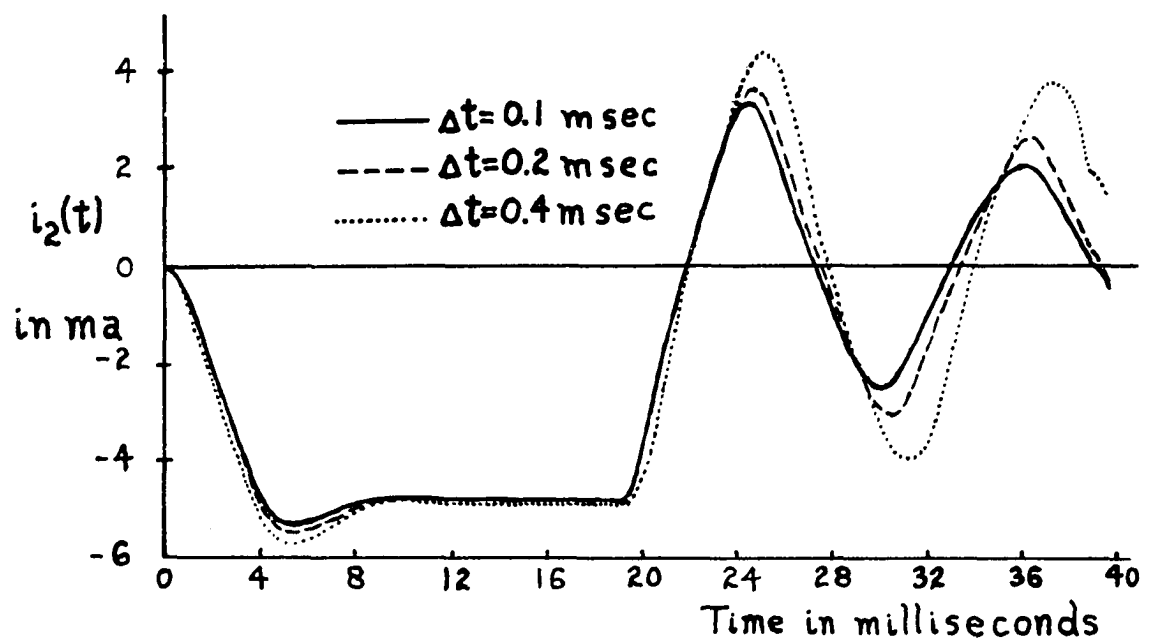

Figure 26. $i_2(t)$ of Figure 22 computed by varying Δt

second half cycle.

The experimental driving voltage, which appears in Figure 21, is observed to be distorted during the first part of the negative half cycle, again due to the low input impedance level encountered at current values of a few milliamperes. The degree of similarity between the wave forms observed and computed is adequate to substantiate that the calculated solution is approximately that of the network posed.

ANALYSIS OF A NONLINEAR FEEDBACK NETWORK

As a final example, a subharmonic generator with the equivalent network of Figure 27 is to be analyzed. This network originates from a thesis by Hughes (4, pp. 4-14) which investigates the second subharmonic content of the output voltage $v_o(t)$. The multiple current sources drive the parallel combination of a nonlinear resistance and a phase shifting sub-network. The latter circuit appears separately in Figure 28. The volt-ampere characteristic of the nonlinear resistance is represented by

$$\begin{aligned} i_{NLR}(t) &\triangleq f(v_o;t) \\ &= 4.765 \times 10^{-6}\left[\operatorname{sgn} v_o(t)\right] \left|v_o(t)\right|^2 . \end{aligned} \tag{70}$$

The current source $g_m e_{g_2}(t)$ represents an external driving function. A direct current $d_3(t)$ flows as a result of the bias conditions on the pentode current generator used. The current source $g_m k v_1(t)$ reflects the fraction k of the output voltage of the phase shifting circuit fed back as a network input. For this example, the symbols of Figures 27 and 28 are identified as

$$\begin{aligned} &e_{g_2}(t) = 0.2 \sin 62{,}800t \text{ volts}, \\ &d_3(t) = 9 \times 10^{-3} \text{ amps}, \\ &g_m = 5{,}000 \text{ microhms}, \\ &k = 0.0781, \end{aligned} \tag{71}$$

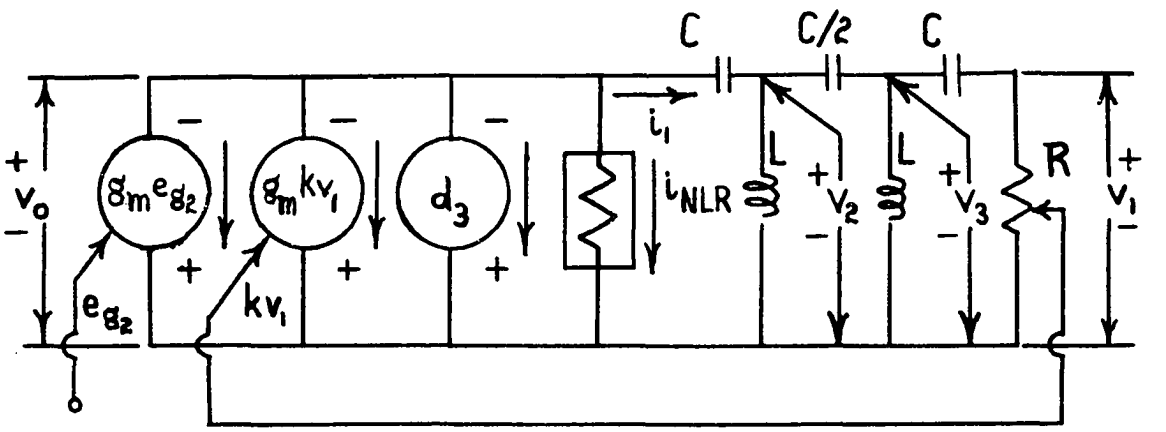

Figure 27. Equivalent circuit for analysis

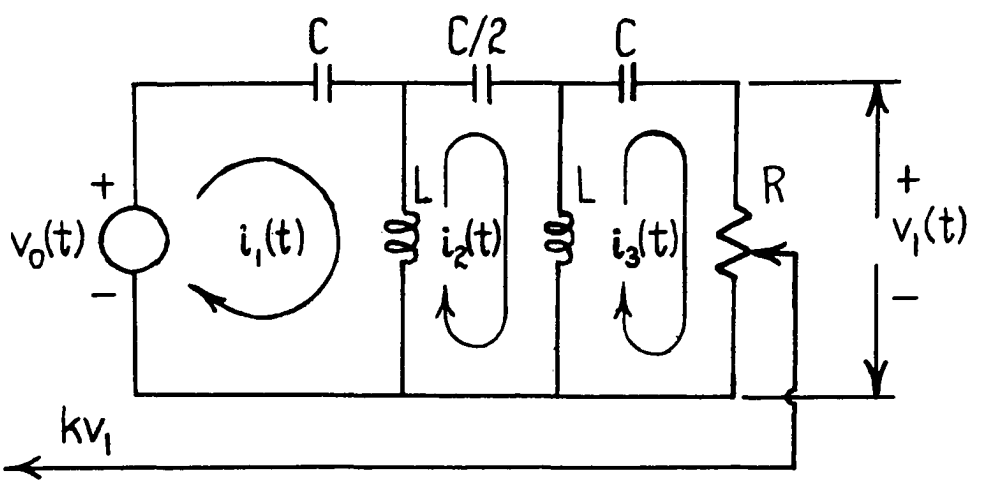

Figure 28. Phase shifting subnetwork of Figure 27

$L = 0.506$ henries,

$R = 0.5 \times 10^{6}$ ohms,

$C = 2 \times 10^{-9}$ farads.

The phase shifting subnetwork is designed to produce a 180° phase shift for a frequency of

$$f = (2\pi\sqrt{LC})^{-1}$$
$$= 5{,}000 \text{ cps} . \qquad (72)$$

for these element values. This frequency corresponds to the second subharmonic of the 10,000 cps frequency of the external driving current.

In the presence of current sources, the node voltage approach is selected for the analysis. For the voltage $v_o(t)$, the following nodal equation is written.

$$-\left[g_m e_{g_2}(t) + d_3(t) + g_m k v_1(t)\right] = i_1(t) + i_{NLR}(t) \qquad (73)$$
$$\triangleq i_1(t) + f(v_o;t) .$$

The nonlinear function $f(v_o;t)$ is now transposed as a pseudo-driving current. Also the linear function of $v_1(t) = Ri_3(t)$ is transposed as an induced current term. With these modifications, equation 73 becomes

$$-\left[g_m e_{g_2}(t) + d_3(t) + f(v_o;t)\right] = i_1(t) + g_m k R i_3(t) . \qquad (74)$$

The currents $i_1(t)$ and $i_3(t)$ are expressed in terms of the dependent variable $v_o(t)$ by a mesh analysis of Figure 28.

To simplify subsequent expressions, define

$$p^n \triangleq \frac{d^n}{dt^n} \text{ for } n \geq 0 ,$$

$$\frac{1}{p} \triangleq \int^t dt . \tag{75}$$

The mesh equations for Figure 28 are then

$$\begin{bmatrix} v_o(t) \\ 0 \\ 0 \end{bmatrix} = \begin{bmatrix} (Lp+\frac{1}{Cp}) & -Lp & 0 \\ -Lp & 2(Lp+\frac{1}{Cp}) & -Lp \\ 0 & -Lp & (Lp+R+\frac{1}{Cp}) \end{bmatrix} \begin{bmatrix} i_1(t) \\ i_2(t) \\ i_3(t) \end{bmatrix} , \tag{76}$$

subject to the initial conditions $i_j(0)$, $q_j(0)$ for $j = 1,2,3$.

In Appendix G, the current transforms for the $I_j(s)$ are derived from equation 76 in terms of the voltage transform $V_o(s)$ and the appropriate initial condition terms. These are

$$\begin{aligned} I_1(s) &= \frac{1}{\Delta'(s)} \Big\{ \big[V_o(s)-B_1(s)\big]\big[L^2C^3s^5+2LRC^3s^4+4LC^2s^3+2RC^2s^2+2Cs\big] \\ &\quad - B_2(s)\big[L^2C^3s^5+LRC^3s^4+LC^2s^3\big] - B_3(s)L^2C^3s^5 \Big\}, \\ I_2(s) &= \frac{1}{\Delta'(s)} \Big\{ \big[V_o(s)-B_1(s)\big]\big[L^2C^3s^5+LRC^3s^4+LC^2s^3\big] \\ &\quad - B_2(s)\big[L^2C^3s^5+LRC^3s^4+2LC^2s^3+RC^2s^2+Cs\big] \\ &\quad - B_3(s)\big[L^2C^3s^5 + LC^2s^3\big] \Big\} , \\ I_3(s) &= \frac{1}{\Delta'(s)} \Big\{ \big[V_o(s)-B_1(s)\big] L^2C^3s^5 - B_2(s)\big[L^2C^3s^5+LC^2s^3\big] \\ &\quad - B_3(s)\big[L^2C^3s^5+ 4LC^2s^3+ 2Cs\big] \Big\} , \end{aligned} \tag{77}$$

where

$$\Delta'(s) = L^2RC^3s^5+4L^2C^2s^4+4LRC^2s^3+6LCs^2+2RCs+ 2 . \tag{78}$$

The initial condition terms are

$$B_1(s) = - L\left[i_1(0) - i_2(0)\right] + \left[sC\right]^{-1}q_1(0) ,$$
$$B_2(s) = - L\left[2i_2(0) - i_1(0) - i_3(0)\right] + 2\left[sC\right]^{-1}q_2(0) , \quad (79)$$
$$B_3(s) = - L\left[i_3(0) - i_2(0)\right] + \left[sC\right]^{-1}q_3(0) .$$

The Laplace transform of equation 74 is

$$- \left[g_m e_{g_2}(t) + d_3(t) + f(v_o;t)\right] = I_1(s) + g_m kRI_3(s) . \quad (80)$$

The expression for $I_1(s)$ and $I_3(s)$ from equation 77 are substituted in equation 80 and the result is solved for the linear occurrence of $V_o(s)$. Upon inverse transformation of this form, the integral equation for iterative solution becomes

$$\begin{aligned} v_o(t) = & - \int_0^t \left[g_m e_{g_2}(\lambda) + d_3(\lambda) + f(v_o;\lambda)\right] P_{00}(t - \lambda)d\lambda \\ & + \int_0^t b_1(\lambda)P_{10}(t - \lambda)d\lambda \\ & + \int_0^t b_2(\lambda)P_{20}(t - \lambda)d\lambda \\ & + \int_0^t b_3(\lambda)P_{30}(t - \lambda)d\lambda \quad . \end{aligned} \quad (81)$$

The quantities of equation 81 are derived in Appendix H for the parameter values specified in equation 71. These are as follow.

$$\begin{aligned} b_1(t) &= -0.506\left[i_1(0)-i_2(0)\right] u_1(t)+0.5\times10^9 q_1(0)u_0(t) \\ b_2(t) &= -0.506\left[2i_2(0)-i_1(0)-i_3(0)\right] u_1(t)+1.0\times10^9 q_2(0)u_0(t) \end{aligned} \quad (82)$$

$$b_3(t) = -0.506\left[i_3(0) - i_2(0)\right]u_1(t) + 0.5\times10^{9}q_3(0)u_0(t)$$

Also,

$$\begin{aligned}
P_{00}(t) &= 2.548\times10^{3}u_1(t)+5.001\times10^{8}u_0(t)-3.408\times10^{8}e^{-2.48\times10^{4}t} \\
&\quad +2.424\times10^{8}e^{7.863\times10^{3}t}\sin(1.842\times10^{4}t-46.19^{0}) , \\
P_{10}(t) &= u_1(t) , \qquad (83) \\
P_{20}(t) &= 99.23e^{-1.001\times10^{3}t}-2.717\times10^{4}e^{-2.48\times10^{4}t} \\
&\quad +2.393\times10^{4}e^{7.863\times10^{3}t}\sin(1.842\times10^{4}t+67.59^{0}) , \\
P_{30}(t) &= 1.955\times10^{5}e^{-1.001\times10^{3}t}-1.417\times10^{5}e^{-2.48\times10^{4}t} \\
&\quad -9.162\times10^{4}e^{7.863\times10^{3}t}\sin(1.842\times10^{4}t+135.96^{0}) .
\end{aligned}$$

The presence of the positive exponential terms is attributed to the value of R selected for this network and indicates a potential instability of the phase shifting subnetwork of Figure 28.

With the $i_j(0)$, $q_j(0)$ specified at some initial time, equation 81 completely describes the variable $v_o(t)$ over some time span $0 \leqslant t \leqslant \tau_u$. If it is desired to extend the solution over additional time spans, it becomes necessary to use an auxiliary set of equations derived from the equation set 76. From the inverse transformation of the equation set 77, the j^{th} current is

$$i_j(t) = \int_0^t P_{1j}(t-\lambda)v_o(\lambda)d\lambda + \sum_{p=1}^{3}\int_0^t P_{pj}(t-\lambda)b_p(\lambda)d\lambda . \qquad (84)$$

Assume that $v_o(t)$ is known for the time span $0 \leq t \leq \tau_u$. Then the initial conditions for the time span $\tau_u \leq t \leq 2\tau_u$ are computed from equation 84 as $i_j(\tau_u)$ and

$$q_j(\tau_u) = q_j(0) + \int_0^{\tau_u} i_j(t)dt \ . \tag{85}$$

The example to be analyzed is posed as follows. Assume that the network is initially in a steady state condition with only the direct current component $d_3(t)$ flowing. The driving current $g_m e_{g_2} \sin \omega t$ is applied at the time origin and the response $v_o(t)$ is to be found for the first time span. The initial conditions are

$$\begin{aligned} i_1(0) &= i_2(0) = i_3(0) = q_2(0) = q_3(0) = 0 \\ q_1(0) &= Cv_o(0) \\ &= C \times 458 \left[\operatorname{sgn} i_{NLR}(0)\right] \left|i_{NLR}(0)\right|^{\frac{1}{2}} \\ &= C \times 458 \left\{\operatorname{sgn}\left[- d_3(0)\right]\right\} \left|d_3(0)\right|^{\frac{1}{2}} \\ &= - 2 \times 10^{-9} \times 458 \times \left[9 \times 10^{-3}\right]^{\frac{1}{2}} \\ &= - 86.9 \times 10^{-9} \ . \end{aligned} \tag{86}$$

With these initial conditions imposed in the definitions of equation 82, all terms of the required integral equation 81 are identified.

The response voltage $v_o(t)$ is presented in Figure 29 for several values of Δt. The steady state frequency and limits of the amplitude of oscillation cannot be predicted on the basis of the coarse calculations made in this

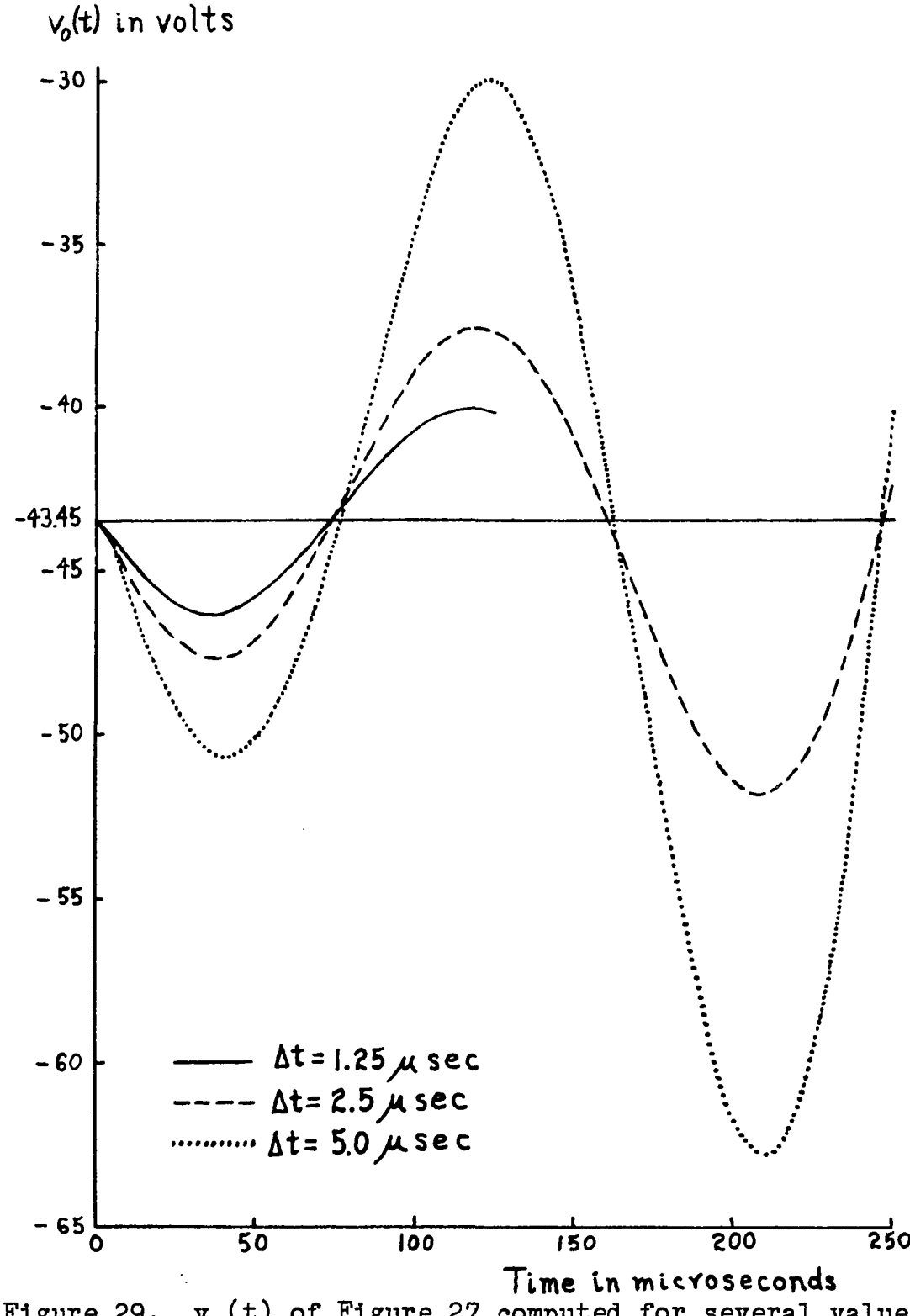

Figure 29. $v_o(t)$ of Figure 27 computed for several values of Δt

transient analysis. However, the observed tendency of the response period to protract itself in time through relatively undistorted oscillation appears to indicate a large percentage of subharmonic content in the response. A period of approximately 150 microseconds is observed in the first oscillation as compared with the source period of 100 microseconds. The contraction of the response amplitude for a greater resolution of Δt does not deny an ultimate instability, but indicates the possibility of a bounded steady state response.

In his thesis, Hughes (4, p. 11) predicts a steady state response of

$$v_o(t) = - 40.9 - 20.48 \sin 31{,}400t \; . \qquad (87)$$

Experimentally this voltage is found to consist of a -40 volt direct current component with a superimposed 18 volt oscillation of the second subharmonic of the driving signal. An harmonic analysis indicates slightly more than one percent distortion in this experimental response.

CONCLUSION

The important results in the development of this method of analysis are summarized as follow.

1. A set of integral equations may be methodically formed for any electrical network for which the mesh or nodal equations may be written.

2. The network may contain multiple nonlinear characteristics if these can be adequately described in terms of the time domain variables of the network.

3. A numerically approximate form of the set of integral equations may be solved by iteration. The proposed iterative method is directly applicable to these approximating forms for the linear occurrence of the dependent variables.

The reliability of the computed transient responses is observed to depend primarily on the resolution of the time increment used. Qualitative information concerning the general waveform of a response is obtained even for a relatively coarse Δt. An accurate determination of the amplitude, frequency and other response characteristics requires a finer resolution of the time increment. In practice, the degree of resolution necessary is determined by observing the sequence of computed responses corresponding to successively smaller values of Δt.

LIST OF REFERENCES

1. Ahlfors, Lars V. Complex analysis. McGraw-Hill Book Co., Inc., New York, N. Y. 1953.

2. Bode, Hendrik W. Network analysis and feedback amplifier design. D. Van Nostrand Company, Inc., Princeton, New Jersey. [c1945].

3. Gardner, Murray F. and Barnes, John L. Transients in linear systems. Vol. 1. John Wiley & Sons, Inc., New York, N. Y. [c1942].

4. Hughes, William Lewis. Stabilization of the locked oscillator frequency divider with nonlinear elements. Unpublished Ph.D. Thesis. Library, Iowa State University of Science and Technology, Ames, Iowa. 1952.

5. Moulton, Forest Ray. Differential equations. Dover Publications, Inc., New York, N. Y. [c1958].

APPENDIX A: THE DEFINITION AND PROPERTIES OF IMPULSES

The unit impulse is to be defined in terms of a rectangular pulse of time duration Δt and amplitude $\frac{1}{\Delta t}$. As Δt approaches zero this pulse retains the property of enclosing unit area. The limit function is defined as the unit impulse. The pulse u(t) may be represented by a sequence of two unit steps, thus

$$u(t) = \frac{1}{\Delta t}\left[u_0(t) - u_0(t - \Delta t)\right] \tag{88}$$

where the unit step $u_0(t)$ is defined by

$$u_0(t) \triangleq \begin{cases} 0 \text{ for } t < 0 \\ 1 \text{ for } t > 0 \end{cases}. \tag{89}$$

The unit impulse is defined as

$$u_1(t) \triangleq \lim_{\Delta t \to 0} \left\{\frac{1}{\Delta t}\left[u_0(t) - u_0(t - \Delta t)\right]\right\}. \tag{90}$$

In accord with the development of transform pairs given in Gardner and Barnes (3, pp. 255-257), equation 88 is transformed as

$$\mathcal{L}\{u(t)\} = \frac{1}{s\Delta t}\left[1 - e^{-s\Delta t}\right] \tag{91}$$

and

$$\mathcal{L}\{u_1(t)\} \triangleq \lim_{\Delta t \to 0} \mathcal{L}\{u(t)\}. \tag{92}$$

This limit is indeterminate, as also that of equation 90, but an application of L'Hospital's rule yields

$$\mathcal{L}\{u_1(t)\} \triangleq \lim_{\Delta t \to 0} e^{-s\Delta t} = 1 \ . \tag{93}$$

The following definition stems from equation 90.

$$u_1(t) \triangleq \frac{du_0(t)}{dt} \tag{94}$$

From equation 94 it follows that

$$\int_{t_1 \leq 0}^{t_2 \geq 0} u_1(t)dt \triangleq u_0(t) \ . \tag{95}$$

Impulses of order higher than the first may be similarly defined. These arise as the limiting cases of unit step sequences whose amplitudes are assigned such that the limits become indeterminate and may be treated as above. For the unit doublet $u_2(t)$, the sequence of unit steps is

$$u(t) = \frac{1}{\Delta t^2}\left[u_0(t) - 2u_0(t - \Delta t) + u_0(t - 2\Delta t)\right] \ . \tag{96}$$

Then

$$\begin{aligned} u_2(t) &\triangleq \lim_{\Delta t \to 0}\left[u(t)\right] \\ &\triangleq \frac{du_1(t)}{dt} \ . \end{aligned} \tag{97}$$

Its transform is

$$\begin{aligned} \mathcal{L}\{u_2(t)\} &= \lim_{\Delta t \to 0}\left\{\frac{1}{s\Delta t^2}\left[1 - 2e^{-s\Delta t} + e^{-2s\Delta t}\right]\right\} \\ &= s \ . \end{aligned} \tag{98}$$

The time integral of the doublet is

$$\int_{t_1 \leq 0}^{t_2 \geq 0} u_2(t)dt \triangleq u_1(t) \ . \tag{99}$$

In general, for an h^{th} order impulse $u_h(t)$, it may be shown that

$$u_h(t) \triangleq \frac{du_{h-1}(t)}{dt} \ , \tag{100a}$$

$$\mathcal{L}\{u_h(t)\} \triangleq s^{h-1} \ , \tag{100b}$$

$$\int_{t_1 \leq 0}^{t_2 \geq 0} u_h(t)dt \triangleq u_{h-1}(t) \ , \tag{100c}$$

for $h \geq 1$.

The time integration of functional products, one factor of which is an impulsive term, is required in the expansion of the solution set of integral equations. It is recalled from Laplace transform theory that

$$\mathcal{L}\left\{\frac{d^n k(t)}{dt^n}\right\} = s^n K(s) - \sum_{i=0}^{n-1} \left.\frac{d^i k(t)}{dt^i}\right|_{t=0} s^{n-1-i} \tag{101}$$

for $n \geq 0$. From the definition of the convolution product and equation 100b

$$\int_0^t u_{n+1}(\lambda)k(t - \lambda)d\lambda = \mathcal{L}^{-1}\left\{s^n K(s)\right\} \ , \tag{102}$$

where $\mathcal{L}\{k(t)\} = K(s)$. By equation 101, this last equality becomes

$$\int_0^t u_{n+1}(\lambda)k(t-\lambda)d\lambda = \frac{d^n k(t)}{dt^n} + \mathcal{L}^{-1}\left\{\sum_{i=0}^{n-1} \left.\frac{d^i k(t)}{dt^i}\right|_{t=0} s^{n-1-i}\right\}$$

$$= \frac{d^n k(t)}{dt^n} + \sum_{i=0}^{n-1} \left.\frac{d^i k(t)}{dt^i}\right|_{t=0} u_{n-1}(t) \ , \tag{103}$$

for $n \geq 0$.

For the cases of greatest interest here,

$$\int_0^t u_1(\lambda)k(t - \lambda)d\lambda = k(t) , \tag{104}$$

$$\int_0^t u_2(\lambda)k(t - \lambda)d\lambda = \frac{dk(t)}{dt} + k(0)u_1(t) . \tag{105}$$

APPENDIX B: CHARACTERISTIC OF THE NONLINEAR RESISTANCE

The nonlinear resistive element is a General Electric thyrite disc clamped between two pieces of sheet brass, electrical contact being made through the latter plates. The experimental volt-ampere characteristic shows negative symmetry with respect to the current origin. Therefore only the data obtained for positive values of current are displayed in Table 1 in addition to certain logarithmic quantities required later for approximation of this characteristic by an assumed functional form.

In Figure 30 appears a logarithmic plot of |e| versus

Table 1. Data for least squares approximation to the nonlinear resistance characteristic

|e|	|i|	log |e|	log |i|	log |e| · log |i|	(log |i|)^2
0	0.00 ma	-	-	-	-
3	0.18 ma	0.478	-3.744	-1.790	14.01
4	0.29 ma	0.602	-3.538	-2.128	12.51
5	0.56 ma	0.698	-3.252	-2.270	10.58
6	0.84 ma	0.778	-3.076	-2.390	9.45
7	1.24 ma	0.845	-2.906	-2.455	8.45
8	1.73 ma	0.903	-2.762	-2.495	7.64
9	2.35 ma	0.954	-2.629	-2.508	6.91
10	3.05 ma	1.000	-2.516	-2.516	6.32
11	3.85 ma	1.042	-2.414	-2.518	5.83
12	4.95 ma	1.078	-2.306	-2.488	5.32
13	6.15 ma	1.114	-2.212	-2.462	4.89
14	7.55 ma	1.146	-2.123	-2.433	4.51
15	9.00 ma	1.176	-2.046	-2.402	4.19
16	10.8 ma	1.204	-1.967	-2.370	3.86
17	13.0 ma	1.230	-1.886	-2.320	3.55
		14.248	-39.377	-35.547	108.02

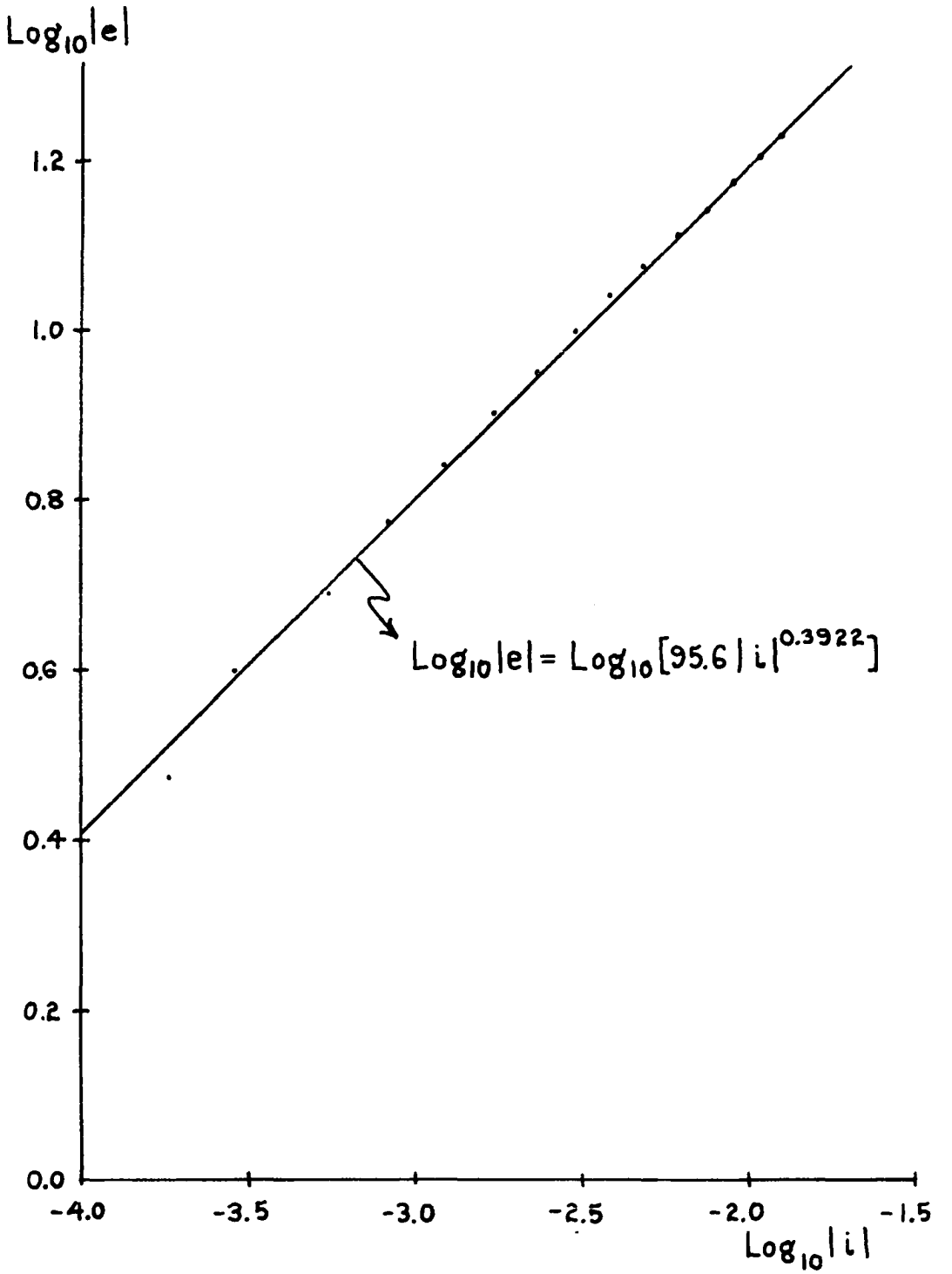

Figure 30. Logarithmic plot of experimental data from Table 1 and the regression line derived therefrom

$|i|$ for these data. The generally linear appearance of this presentation leads to the assumption that the volt-ampere relationship may be approximated by

$$|e| = K|i|^n , \tag{106}$$

or for signed current values

$$e = K(\operatorname{sgn} i)|i|^n . \tag{107}$$

The coefficients K and n are obtained by determining a line of best fit by the least squares criteria to the log $|e|$ versus log $|i|$ data appearing in Table 1. All logarithms appearing in this appendix are assumed to be common logarithms.

The linear regression form is obtained by taking the common logarithm of equation 106, thus

$$\log |e| = \log K + n \log |i| \tag{108}$$

The coefficients K and n are determined as

$$\log K = \frac{\sum_{j=1}^{N} \log |e_j| \sum_{k=1}^{N} (\log |i_k|)^2 - \sum_{j=1}^{N} \log |i_j| \sum_{k=1}^{N} \log |i_k| \cdot \log |e_k|}{N \sum_{j=1}^{N} (\log |i_j|)^2 - (\sum_{j=1}^{N} \log |i_j|)^2} , \tag{109}$$

$$n = \frac{N \sum_{j=1}^{N} \log |i_j| \cdot \log |e_j| - \sum_{j=1}^{N} \log |i_j| \sum_{k=1}^{N} \log |e_k|}{N \sum_{j=1}^{N} (\log |i_j|)^2 - (\sum_{j=1}^{N} \log |i_j|)^2} \tag{110}$$

where N is the number of samples to be considered.

For the case at hand involving the 15 nonzero entries of Table 1,

$$K \doteq \text{antilog } 1.98 = 95.6 \qquad (111)$$

$$n \doteq 0.392$$

where the ($\doteq$) denotes the use of slide rule calculations for the data processing involved. In Figure 31 is presented a comparison of the approximating function so selected and the experimental data which it represents.

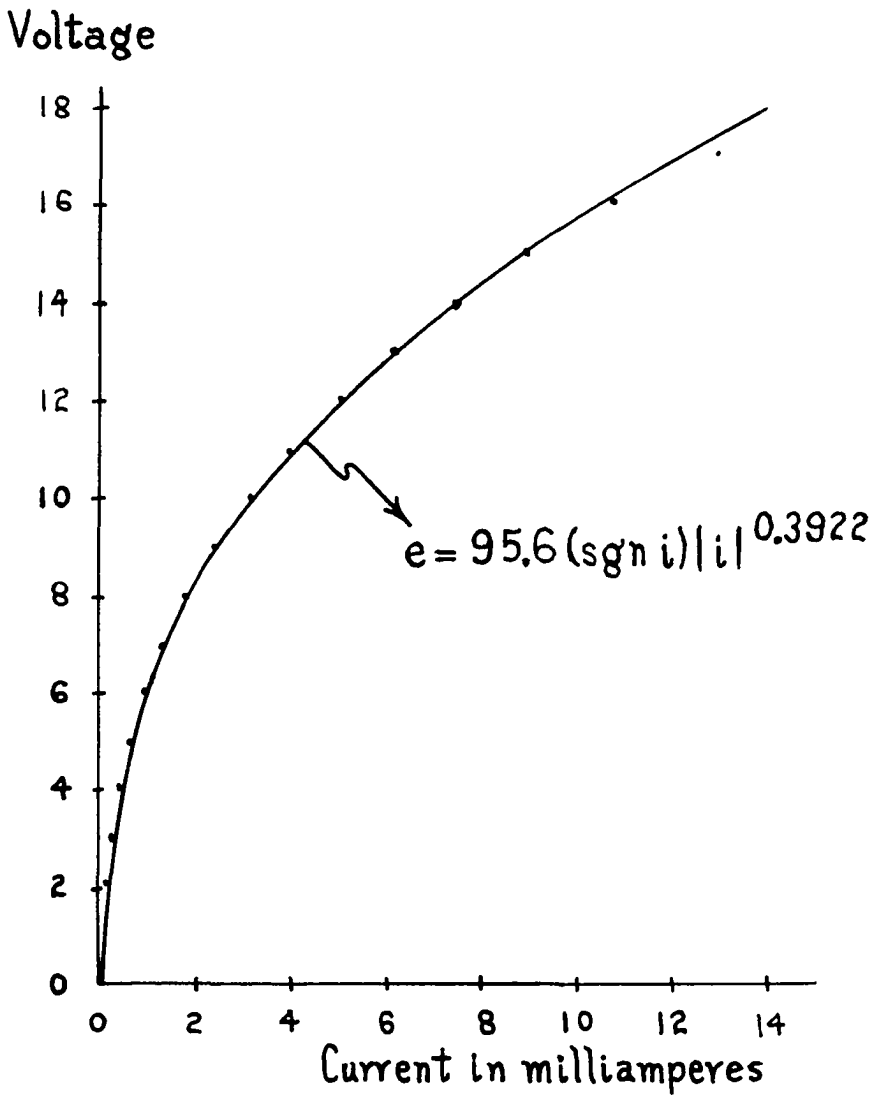

Figure 31. Comparison of the experimental data of Table 1 and its approximating function

APPENDIX C: CHARACTERISTIC OF THE NONLINEAR INDUCTANCE

The nonlinear inductive characteristic is obtained by driving an iron core transformer into saturation. From the flux-current characteristic of this element, the desired volt-ampere characteristic is derived by Lenz's law. Thus

$$e = \frac{d\lambda(i)}{dt} = \frac{d\lambda(i)}{di}\frac{di}{dt}, \qquad (112)$$

where $\lambda(i)$ describes the induced magnetic flux as a function of the exciting current. In the latter form, the term $\frac{d\lambda(i)}{di}$ is defined as the incremental inductance of the element. This is recognized as the constant L in the case of an inductance operating in its linear range. For this treatment, the intermediate form of equation 112 is to be used since only the single approximation

$$\frac{\Delta\lambda(i)}{\Delta t} \doteq \frac{d\lambda(i)}{dt} \qquad (113)$$

is necessary. To obtain the λ versus i characteristic of Figures 32 and 33, the time integral of the voltage induced across the inductance by a sinusoidal source is plotted on an oscilloscope against a voltage proportional to the current through the element.

In Figure 32 are presented the family of hysteresis loops for the saturating element. The mean magnetization curve which is estimated from this family appears as a dashed line. Also included are two straight lines which represent

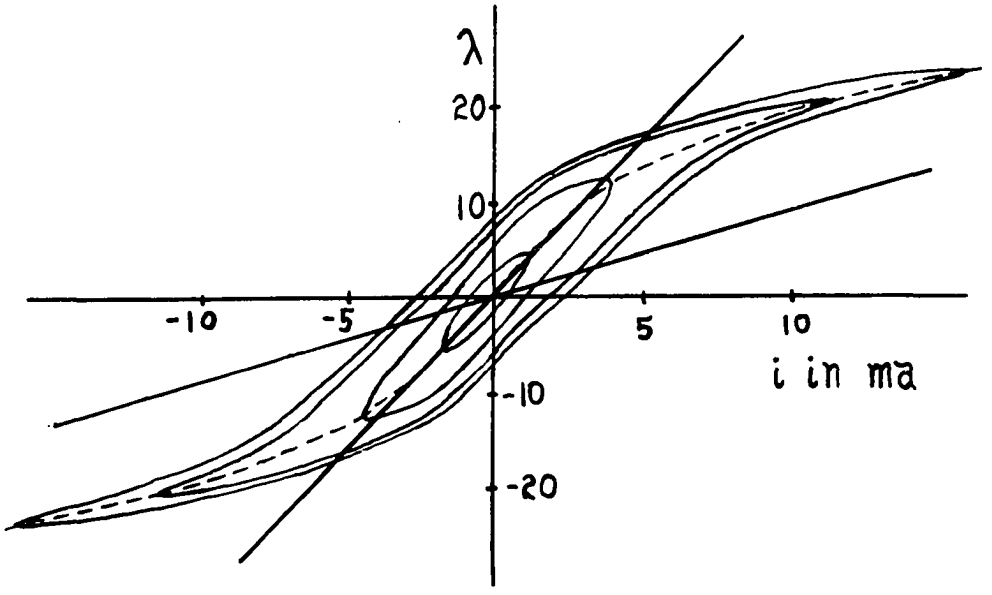

Figure 32. Magnetization curves for a saturable element with unbiased excitation

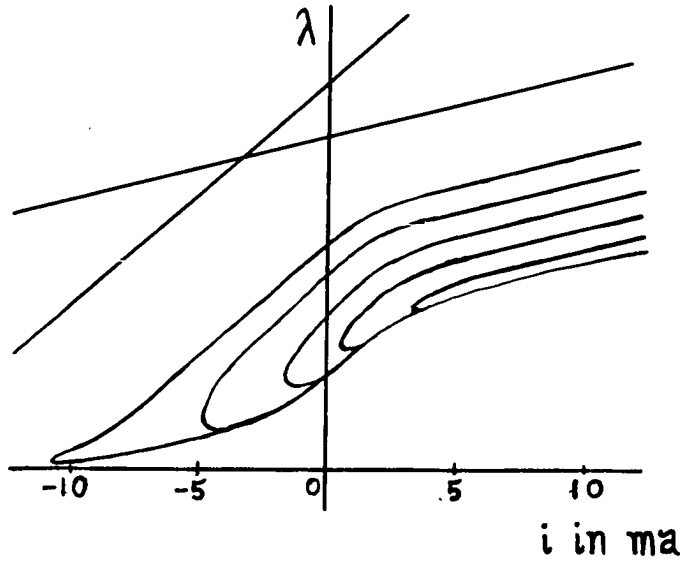

Figure 33. Magnetization curves for the element of Figure 32 with biased excitation

the assumed upper and lower bounds on the slope of the hysteresis curves. These lines are introduced by replacing the saturable element with a calibrated decade box of low hysteresis coils operating in their region of linearity. Figure 33 presents the family of hysteresis loops produced by a variable amplitude sinusoid superimposed on a constant direct current bias voltage. The lines representing upper and lower bounds on the slope of the hysteresis curves of Figure 32 are included to assist in comparing these two figures.

Although the hysteresis present in Figure 32 is not inconsiderable, its effects are to be excluded. The following segmented approximation is made to the mean magnetization curve observed.

$$\lambda_1 = k_1 i$$

for $0 \leq |i| \leq i_{m_1}$,

$$\lambda_2 = (\text{sgn } i)\left[k_2 i^2 + k_3 |i| + k_4\right]$$

for $i_{m_1} \leq |i| \leq i_{m_2}$, (114)

$$\lambda_3 = (\text{sgn } i)\left\{\lambda_2(i_{m_2}) + k_5\left[|i| - i_{m_2}\right]\right\}$$

for $i_{m_2} \leq |i|$.

To assign the appropriate coefficients, k_1 is determined graphically as the slope of the low current parallel of Figure 32; k_5 as the slope of the parallel for large current

values; k_2, k_3, k_4 as the coefficients of a second degree polynomial approximating the smooth curve joining the straight line segments of the mean magnetization curve. The polynomial coefficients are obtained by requiring that the quadratic pass through an assigned intersection with each of the two parallels and an intermediate point selected by observation. The points so selected are

$$\begin{aligned}(\lambda, i): &(6.6 \times 10^{-3},\ 2.0 \times 10^{-3}) \\ &(14.5 \times 10^{-3},\ 6.36 \times 10^{-3}) \\ &(19.2 \times 10^{-3},\ 10.0 \times 10^{-3})\end{aligned} \tag{115}$$

The solution of the set of three simultaneous equations obtained by substituting a different point pair in the assumed quadratic form for each, results in the coefficient determination.

For the element considered, the segmented approximation is

$$\lambda_1 = 3.3i$$

for $0 \leq |i| \leq 2.0 \times 10^{-3}$,

$$\lambda_2 = (\text{sgn } i)\left[-67.5|i|^2 + 2.398|i| + 1.973 \times 10^{-3}\right]$$

for $2.0 \times 10^{-3} \leq |i| \leq 10.0 \times 10^{-3}$, (116)

$$\lambda_3 = (\text{sgn } i)\left\{19.2 \times 10^{-3} + 0.935\left[|i| - 10.0 \times 10^{-3}\right]\right\}$$

for $10.0 \times 10^{-3} \leq |i|$.

Although no attempt has been made to include the hysteresis effects of the saturable element in the approximat-

ing form of the flux-current characteristics, certain aspects of these effects in Figures 32 and 33 are of interest. For the unbiased hysteresis family of Figure 32, there exists an incremental inductance versus current family similar to that shown in Figure 34. The values of slope of the low and high current parallels appear to serve as upper and lower bounds respectively. The existence of a positive lower bound for the incremental inductance of a passive element is consistent with physical reasoning.

Figure 35 represents the incremental inductance versus current family roughly estimated from Figure 33. It is interesting to note the discontinuity in incremental inductance which occurs in several of these loops for the biased excitation.

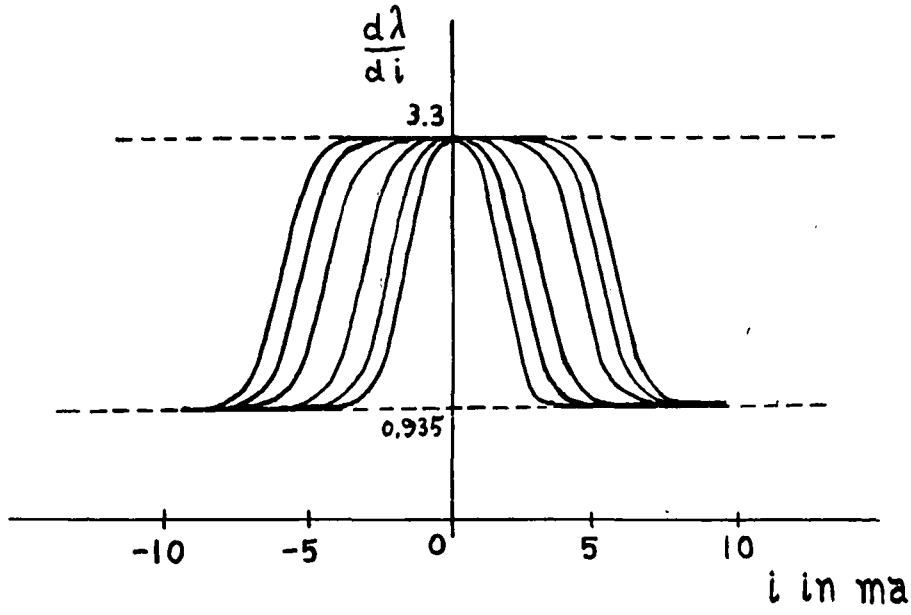

Figure 34. Incremental inductance versus current derived approximately from Figure 32

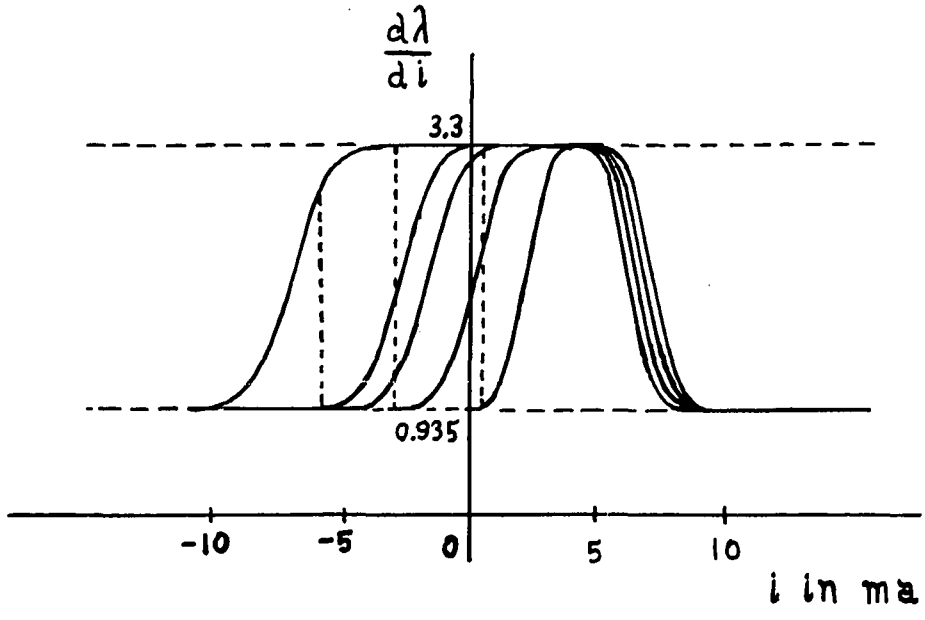

Figure 35. Incremental inductance versus current derived approximately from Figure 33

APPENDIX D: GENERAL ADMITTANCE AND INITIAL CONDITION TRANSFORMS OF THE TWO MESH NETWORK FOR SAMPLE ANALYSIS

Consider the following network and the set of mesh equations describing it.

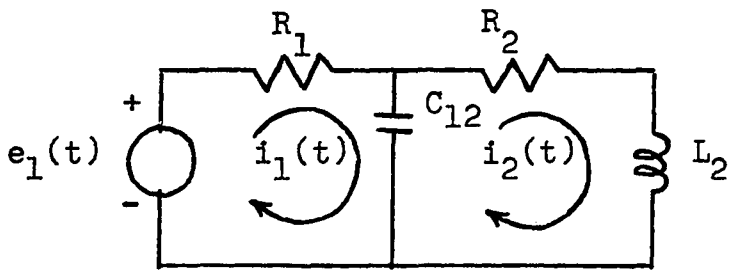

$$e_1(t) = \left[R_1 + C_{12}^{-1}\int dt\right]i_1(t) - \left[C_{12}^{-1}\int dt\right]i_2(t)$$

$$0 = -\left[C_{12}^{-1}\int dt\right]i_1(t) + \left[L_2\frac{d}{dt} + R_2 + C_{12}^{-1}\int dt\right]i_2(t) .$$

Upon Laplace transformation and with the initial condition terms treated as driving voltages, these appear in matrix form as

$$\begin{vmatrix} E_1(s) - \frac{1}{sC_{12}}\left[q_1(0) - q_2(0)\right] \\ L_2 i_2(0) - \frac{1}{sC_{12}}\left[q_2(0) - q_1(0)\right] \end{vmatrix} = \begin{bmatrix} \left[R_1 + \frac{1}{sC_{12}}\right] & \left[-\frac{1}{sC_{12}}\right] \\ \left[-\frac{1}{sC_{12}}\right] & \left[sL_2 + R_2 + \frac{1}{sC_{12}}\right] \end{bmatrix} \begin{vmatrix} I_1(s) \\ I_2(s) \end{vmatrix} .$$

For this equation set,

$$\Delta(s) = \left(R_1 + \frac{1}{sC_{12}}\right)\left(sL_2 + R_2 + \frac{1}{sC_{12}}\right) - \left(\frac{1}{sC_{12}}\right)^2$$

$$= \frac{R_1 L_2}{s}\left(s^2 + A_1 s + A_2\right) ,$$

where

$$A_1 = \frac{R_1R_2C_{12} + L_2}{R_1L_2C_{12}} ,$$

$$A_2 = \frac{R_1 + R_2}{R_1L_2C_{12}} .$$

The admittance transforms are the signed cofactors

$$\frac{\Delta_{11}(s)}{\Delta(s)} = \frac{sL_2 + R_2 + \frac{1}{sC_{12}}}{\Delta(s)}$$

$$= \frac{1}{R_1}\left[\frac{s^2 + \frac{R_2}{L_2}s + \frac{1}{L_2C_{12}}}{s^2 + A_1s + A_2}\right],$$

$$\frac{\Delta_{12}(s)}{\Delta(s)} = \frac{\Delta_{21}(s)}{\Delta(s)} = \frac{1}{sC_{12}\Delta(s)}$$

$$= \frac{1}{L_2R_1C_{12}}\left(\frac{1}{s^2 + A_1s + A_2}\right) ,$$

$$\frac{\Delta_{22}(s)}{\Delta(s)} = \frac{R_1 + \frac{1}{sC_{12}}}{\Delta(s)}$$

$$= \frac{1}{L_2}\left[\frac{s + \frac{1}{R_1C_{12}}}{s^2 + A_1s + A_2}\right] .$$

The initial condition transforms are

$$B_1(s) = \frac{1}{sC_{12}}\left[q_1(0) - q_2(0)\right] ,$$

$$B_2(s) = -L_2i_2(0) + \frac{1}{sC_{12}}\left[q_2(0) - q_1(0)\right] .$$

APPENDIX E: ADMITTANCE AND INITIAL CONDITION FUNCTIONS FOR THE TWO MESH NETWORK INCLUDING A NONLINEAR RESISTANCE

Consider the network of Appendix D as the linear portion of the network for this analysis. The parameter values are assigned as

$$R_1 = 1253.2\ \Omega,$$
$$R_2 = 50.6\ \Omega,$$
$$L_2 = 1.0\ \text{h},$$
$$C_{12} = 1.0\ \mu\text{f}.$$

The admittance functions are derived from the admittance transforms of Appendix D as follow.

$$\frac{\Delta_{11}(s)}{\Delta(s)} = \frac{1}{1253.2}\left(\frac{s^2 + 50.6s + 1 \times 10^6}{s^2 + 848.6s + 1.04 \times 10^6}\right)$$

$$= 0.798 \times 10^{-3}\left[1 - 798.0\left(\frac{s + 50.6}{s^2 + 848.6s + 1.04 \times 10^6}\right)\right],$$

then

$$P_{11}(t) = \mathcal{L}^{-1}\left\{\frac{\Delta_{11}(s)}{\Delta(s)}\right\}$$

$$= 0.798 \times 10^{-3}u_1(t) + 0.686e^{-424.3t}\sin(927t - 1.19).$$

$$\frac{\Delta_{12}(s)}{\Delta(s)} = \frac{\Delta_{21}(s)}{\Delta(s)} = \frac{1}{1253.2}\left(\frac{1}{s^2 + 848.6s + 1.04 \times 10^6}\right),$$

then

$$P_{12}(t) = P_{21}(t) = \mathcal{L}^{-1}\left\{\frac{\Delta_{12}(s)}{\Delta(s)}\right\}$$

$$= 0.861e^{-424.3t}\sin(927t).$$

$$\frac{\Delta_{22}(s)}{\Delta(s)} = \left(\frac{s + 798.0}{s^2 + 848.6s + 1.04 \times 10^6}\right) ,$$

then

$$P_{22}(t) = \mathcal{L}^{-1}\left\{\frac{\Delta_{22}(s)}{\Delta(s)}\right\}$$

$$= 1.079e^{-424.3t}\sin(927t + 1.19) .$$

The initial condition terms similarly follow from the forms of Appendix D for these parameter values.

$$b_1(t) = \mathcal{L}^{-1}\{B_1(s)\}$$

$$= 1 \times 10^6\left[q_1(0) - q_2(0)\right]u_0(t) .$$

$$b_2(t) = \mathcal{L}^{-1}\{B_2(s)\}$$

$$= -1.0\, i_2(0)u_1(t) + 1 \times 10^6\left[q_2(0) - q_1(0)\right]u_0(t) .$$

APPENDIX F: ADMITTANCE AND INITIAL CONDITION FUNCTIONS FOR THE TWO MESH NETWORK INCLUDING A NONLINEAR INDUCTANCE

Consider the network of Appendix D as the linear portion of the network for this analysis. The parameter values are assigned as

$$R_1 = 1253.2\ \Omega,$$
$$R_2 = 67.5\ \Omega,$$
$$L_2 = 3.3\ \text{h},$$
$$C_{12} = 1.0\ \mu\text{f}.$$

The admittance functions are derived from the admittance transforms of Appendix D as follow.

$$\frac{\Delta_{11}(s)}{\Delta(s)} = \frac{1}{1253.2}\left(\frac{s^2 + 20.49s + 0.303 \times 10^6}{s^2 + 818.45s + 0.31937 \times 10^6}\right)$$

$$= 0.798 \times 10^{-3}\left[1 - 798.0\left(\frac{s + 20.49}{s^2+818.45s+0.31937\times10^6}\right)\right],$$

then

$$P_{11}(t) = \mathcal{L}^{-1}\left\{\frac{\Delta_{11}(s)}{\Delta(s)}\right\}$$

$$= 0.798 \times 10^{-3}u_1(t) + 0.900e^{-409.23t}\sin(389.75t-0.788).$$

$$\frac{\Delta_{12}(s)}{\Delta(s)} = \frac{\Delta_{21}(s)}{\Delta(s)} = \frac{1}{3.3\times1253.2}\left(\frac{1}{s^2+ 818.45s+0.31937\times10^6}\right),$$

then

$$P_{12}(t) = P_{21}(t) = \mathcal{L}^{-1}\left\{\frac{\Delta_{12}(s)}{\Delta(s)}\right\}$$

$$= 0.620e^{-409.23t}\sin(389.75t).$$

$$\frac{\Delta_{22}(s)}{\Delta(s)} = \frac{1}{3.3}\left(\frac{s + 797.96}{s^2 + 818.45s + 0.31937 \times 10^6}\right) ,$$

then

$$P_{22}(t) = \mathcal{L}^{-1}\left\{\frac{\Delta_{22}(s)}{\Delta(s)}\right\}$$

$$= 0.428e^{-409.23t}\sin(389.75t + 0.788) .$$

The initial condition terms similarly follow from the forms of Appendix D for these parameter values.

$$b_1(t) = \mathcal{L}^{-1}\{B_1(s)\}$$

$$= 1 \times 10^6\left[q_1(0) - q_2(0)\right] u_0(t) .$$

$$b_2(t) = \mathcal{L}^{-1}\{B_2(s)\}$$

$$= - 3.3i_2(0)u_1(t) + 1 \times 10^6\left[q_2(0) - q_1(0)\right] u_0(t) .$$

APPENDIX G: DEVELOPMENT OF CURRENT AND INITIAL CONDITION TRANSFORMS FOR EQUATION 76

The Laplace transform of equation 76 is

$$\begin{bmatrix} V_0(s) \\ 0 \\ 0 \end{bmatrix} = \begin{bmatrix} (sL + \frac{1}{sC}) & (-sL) & 0 \\ (-sL) & 2(sL + \frac{1}{sC}) & (-sL) \\ 0 & (-sL) & (sL + R + \frac{1}{sC}) \end{bmatrix} \begin{bmatrix} I_1(s) \\ I_2(s) \\ I_3(s) \end{bmatrix} + \begin{bmatrix} B_1(s) \\ B_2(s) \\ B_3(s) \end{bmatrix}$$

where the $B_i(s)$ are

$$B_1(s) = - L\left[i_1(0) - i_2(0)\right] + (sC)^{-1}q_1(0) ,$$
$$B_2(s) = - L\left[2i_2(0) - i_1(0) - i_3(0)\right] + 2(sC)^{-1}q_2(0) ,$$
$$B_3(s) = - L\left[i_3(0) - i_2(0)\right] + (sC)^{-1}q_3(0) .$$

With the $B_i(s)$ transposed as psuedo-driving voltages,

$$\Delta(s) = (sL+ \tfrac{1}{sC})\left[2(sL+ \tfrac{1}{sC})(sL+R+ \tfrac{1}{sC})-s^2L^2\right]-s^2L^2(sL+R+ \tfrac{1}{sC})$$
$$= \frac{1}{s^3C^3} (L^2RC^3s^5+ 4L^2C^2s^4+ 4LRC^2s^3+ 6LCs^2+ 2RCs + 2)$$
$$= \frac{\Delta'(s)}{s^3C^3} ,$$

$$I_1(s) = \frac{1}{\Delta'(s)}\Big\{\left[V_0(s)-B_1(s)\right]\left[L^2C^3s^5+2LRC^3s^4+4LC^2s^3+2RC^2s^2+2Cs\right]$$
$$- B_2(s)\left[L^2C^3s^5+LRC^3s^4+ LC^2s^3\right] - B_3(s)L^2C^3s^5\Big\},$$

$$I_2(s) = \frac{1}{\Delta'(s)}\Big\{\left[V_0(s) - B_1(s)\right]\left[L^2C^3s^5+ LRC^3s^4+ LC^2s^3\right]$$
$$- B_2(s)\left[L^2C^3s^5+ LRC^3s^4+ 2LC^2s^3+ RC^2s^2+ Cs\right]$$
$$- B_3(s)\left[L^2C^3s^5+ LC^2s^3\right]\Big\},$$

$$I_3(s) = \frac{1}{\Delta'(s)}\Big\{\big[V_0(s) - B_1(s)\big] L^2C^3s^5 - B_2(s)\big[L^2C^3s^5 + LC^2s^3\big] - B_3(s)\big[L^2C^3s^5 + 4LC^2s^3 + 2Cs\big]\Big\}.$$

APPENDIX H: DEVELOPMENT OF EQUATIONS 82 AND 83

Substitution from equation 77 into equation 80 produces

$$\Delta'(s)\left[-g_m E_{g_2}(s) - D_3(s) - F(V_0;s)\right] =$$
$$\left[V_0(s)-B_1(s)\right]\left[(1+g_m kR)L^2C^3s^5+2LRC^3s^4+4LC^2s^3+2RC^2s^2+2Cs\right]$$
$$- B_2(s)\left[(1+g_m kR)L^2C^3s^5+ LRC^3s^4+ (1+g_m kR)LC^2s^3\right]$$
$$- B_3(s)\left[(1+g_m kR)L^2C^3s^5+ 4g_m kRLC^2s^3+ 2g_m kRCs\right].$$

Define

$$\overline{\Delta}(s) = (1+g_m kR)L^2C^3s^5+ 2LRC^3s^4+ 4LC^2s^3+ 2RC^2s^2+ 2Cs \quad .$$

The first equation above is solved for the linear occurrence of $V_0(s)$, thus

$$V_0(s) = \mathcal{L}\{P_{00}(t)\}\left[-g_m E_{g_2}(s) - D_3(s) - F(V_0;s)\right]$$
$$+\mathcal{L}\{P_{10}(t)\}B_1(s) +\mathcal{L}\{P_{20}(t)\}B_2(s)+\mathcal{L}\{P_{30}(t)\}B_3(s)$$

where

$$\mathcal{L}\{P_{00}(t)\} \triangleq \frac{\Delta'(s)}{\overline{\Delta}(s)} ,$$

$$\mathcal{L}\{P_{10}(t)\} \triangleq 1 ,$$

$$\mathcal{L}\{P_{20}(t)\} \triangleq \frac{1}{\overline{\Delta}(s)}\left[(1+g_m kR)L^2C^3s^5+LRC^3s^4+(1+g_m kR)LC^2s^3\right] ,$$

$$\mathcal{L}\{P_{30}(t)\} \triangleq \frac{1}{\overline{\Delta}(s)}\left[(1+g_m kR)L^2C^3s^5+4g_m kRLC^2s^3+2g_m kRCs\right] ,$$

and

$$\overline{\Delta}(s) \triangleq (1 + g_m kR)L^2C^3s^5+ 2LRC^3s^4+ 4LC^2s^3+ 2RC^2s^2+ 2Cs \quad .$$

For the parameter values assigned by equation 71, the quantities required in the expression for $V_0(s)$ are

$$\overline{\Delta}(s) = 4.019 \times 10^{-25}(s^5 + 1.007\times10^4 s^4 + 2.014\times10^7 s^3 + 0.995 \times 10^{13} s^2 + 0.995 \times 10^{16} s) ,$$

$$\Delta'(s) = 1.024 \times 10^{-21}(s^5 + 4.0 \times 10^3 s^4 + 3.953 \times 10^9 s^3 + 5.929 \times 10^{12} s^2 + 1.953 \times 10^{18} s + 1.953 \times 10^{21}) ,$$

$$\mathcal{L}\{P_{20}(t)\} = \frac{1}{\overline{\Delta}(s)} 4.019\times10^{-25}(s^5+5.035\times10^3 s^4+9.881\times10^8 s^3) ,$$

$$\mathcal{L}\{P_{30}(t)\} = \frac{1}{\overline{\Delta}(s)} 4.019\times10^{-25}(s^5+3.932\times10^9 s^3+1.943\times10^{18} s) .$$

The roots of the polynomial $\overline{\Delta}(s)$ are approximately

$$s_1 = 0 ,$$
$$s_2 = -1.001 \times 10^3 ,$$
$$s_3 = -2.480 \times 10^4 ,$$
$$s_4 = 7.863 \times 10^3 + j1.842 \times 10^4 ,$$
$$s_5 = 7.863 \times 10^3 - j1.842 \times 10^4 .$$

The functions $P_{p0}(t)$ are obtained from their transforms above as

$$P_{00}(t) = 2.548\times10^3 u_1(t)+5.001\times10^8 u_0(t)-3.408\times10^8 e^{-2.48\times10^4 t} + 2.424\times10^8 e^{7.863\times10^3 t}\sin(1.842\times10^4 t - 46.19^\circ) ,$$

$$P_{10}(t) = u_1(t) ,$$

$$P_{20}(t) = 99.23e^{-1.001\times10^3 t} - 2.717\times10^4 e^{-2.48\times10^4 t} + 2.393\times10^4 e^{7.863\times10^3 t}\sin(1.842\times10^4 t + 67.59^\circ) ,$$

$$P_{30}(t) = 1.955\text{x}10^{5}e^{-1.001\text{x}10^{3}t} - 1.417\text{x}10^{5}e^{-2.48\text{x}10^{4}t} - 9.162\text{x}10^{4}e^{7.863\text{x}10^{3}t}\sin(1.842\text{x}10^{4}t + 135.96^{\circ}) .$$

Also the $b_p(t)$ become

$$b_1(t) = -0.506\left[i_1(0) - i_2(0)\right]u_1(t) + 0.5 \times 10^{9}q_1(0)u_0(t) ,$$

$$b_2(t) = -0.506\left[2i_2(0) - i_1(0) - i_3(0)\right]u_1(t) + 1.0\text{x}10^{9}q_2(0)u_0(t) ,$$

$$b_3(t) = -0.506\left[i_3(0) - i_2(0)\right]u_1(t) + 0.5 \times 10^{9}q_3(0)u_0(t) .$$